SIMULATION STUDY OF LIGHTNING FAULT WAVEFORMS INFLUENCED BY THE ARC QUENCHING PROPERTIES OF WOODEN DISTRIBUTION LINE POLES

Carl Henk Bredenoord

A dissertation submitted to the faculty of Engineering and the Built Environment, University of the Witwatersrand, Johannesburg, in part fulfilment of the requirements for the degree of Master of Science in Engineering.

17 May 2006

Declaration

I declare that this dissertation is my own, unaided work, except where otherwise acknowledged. It is being submitted in part fulfilment of the degree of Master in Science in Engineering in the University of the Witwatersrand, Johannesburg. It has not been submitted before for any degree or examination in any other university.

Signed this _____ day of _____ 20____

_____
Carl Henk Bredenoord

Abstract

With an ever increasing emphasis on reliability of supply, improvement in the lightning performance of distribution lines is required. The arc quenching properties of wooden distribution line poles during lightning strikes are an important factor in the reduction of switchgear operation, hence outages. Measurements were conducted on a 22 kV distribution line and it was suspected, in some cases, that direct lightning strikes to the line did not cause switchgear operation. Distribution lines predominantly use wooden poles with a specific configuration which incorporates a 'wooden' spark gap. This paper provides background to the basic configuration of a typical distribution line and the processes which govern the electric arc. A simulation using a dynamic arc model shows that field measured lightning overvoltages on a distribution line are reproducible through system modelling. The simplistic dynamic arc model developed is sufficiently accurate to describe a set of arcs in a larger system such as a distribution line.

This work is dedicated to my Mother and Father, thank you for all your love and support.

Acknowledgements

CONTENTS

LIST OF FIGURES

SIMULATION STUDY OF LIGHTNING FAULT WAVEFORMS INFLUENCED BY THE ARC QUENCHING PROPERTIES OF WOODEN DISTRIBUTION LINE POLES

Carl Henk Bredenoord

Abstract— With an ever increasing emphasis on reliability of supply, improvement in the lightning performance of distribution lines is required. The arc quenching properties of wooden distribution line poles during lightning strikes are an important factor in the reduction of switchgear operation, hence outages. Measurements were conducted on a 22 kV distribution line and it was suspected, in some cases, that direct lightning strikes to the line did not cause switchgear operation. Distribution lines predominantly use wooden poles with a specific configuration which incorporates a 'wooden' spark gap. This paper provides background to the basic configuration of a typical distribution line and the processes which govern the electric arc. A simulation using a dynamic arc model shows that field measured lightning over-voltages on a distribution line are reproducible through system modelling. The simplistic dynamic arc model developed is sufficiently accurate to describe a set of arcs in a larger system such as a distribution line.

Index Terms— Arc quenching, wood, distribution, protection, lightning, 22 kV.

I. INTRODUCTION

THE purpose of the research was to present a simulation model of the arc quenching properties of wood. The field specifically investigated was that of wooden distribution line poles. Wood poles are commonly used due to availability, and with correct configuration are more resistant to lightning strokes than concrete or metal poles.

The development of the arc model was based on data obtained from literature on arc quenching, surface arcing, breaker arc quenching, and simplified plasma physics. Initially a distribution line model with no arc quenching was developed in the simulation package ATP-EMTP (Electromagnetic Transients program) [1]. Due to the many unknown factors in the arc model development it was important to ensure that the distribution line model was accurate. Once a basic model was developed, it was possible to implement a static resistance arc quenching model. Through simulation and comparison with field measurements (obtained from Eskom) it was possible to create a dynamic resistance arc simulation model which roughly modeled the arc quenching properties of wood. In each phase of the development an attempt was made to maintain a degree of simplicity which aided in understanding the processes involved and reduced probability of error.

II. DISTRIBUTION LINE MODEL

This section discusses the development of a distribution line model implemented in ATP-EMTP and provides background information about the different 'components' of the line. Each subsection discusses a part of the line. Finally all the segments are combined and a brief analysis of initial simulation data is presented.

In the line design process, three disturbance criteria are important to consider:
- Maximum system operating voltages (50 Hz).
- Temporary supply frequency over-voltages.
- Lightning impulse voltages (direct & indirect).

Most of the new distribution networks operate at a nominal line voltage of 22 kV. Thus the highest expected line voltage is 24 kV and the lightning impulse withstand voltage of equipment is 150 kV [2].

In determining the performance and appropriate impulse insulation level certain factors need to be considered:
- The withstand tolerance of the equipment to be connected to the network.
- The positioning and number of protective devices.
- Shielding.
- Soil resistance and grounding arrangement.
- The statistical occurrence of impulse overvoltages for the area.

A. Direct Lightning Strikes

The probability of a direct strike depends on the:
- Ground flash density.
- Line length.
- Line height.
- Degree of line shielding by adjacent objects such as trees.

Lightning current has a characteristic fast rise time; hence the voltage on overhead conductors rises very quickly after a direct strike. Negative downward lightning first strokes have a median 5,5/75 μs waveform while subsequent strokes have a median 1,1/32 μs waveform [3].

Direct strikes to unshielded lines result in a flashover to other phases and to ground. If the insulation levels are low (< 100 kV) there will be flashover at several of the poles. The number of poles affected depends on the pole footing resistance. If the insulation levels are high (> 1 MV) then flashover may only occur at a single pole (or not at all). In the event of no flashover, severe surge voltage and currents are transmitted to equipment connected to the line.

If flashover results in a power frequency arc, and there is no arc quenching mechanism, the line needs to be tripped and then restored after a short settling period. The time between tripping the line and re-closing is termed the dead time. Auto-reclosure needs to take into account the time duration of multiple strokes. A dead time of 1 second is generally sufficient [4].

A direct strike may cause damage to a pole in the form of surface splintering, or worst case, complete shattering. The depth of penetration of the arc into the wood will determine the degree of damage. Wood species is an important factor with the penetration of bolts as a secondary factor [5].

The source used for simulations is of Type 15 - Heidler Source. The Heidler source allows the user to specify the approximate magnitude, front duration and stroke duration of the surge. The magnitude of the source was 35 kA, front time was set as 5.6 μs, and the stroke duration as 75 μs.

B. Indirect Lightning Strikes

Close proximity strikes induce voltages on MV lines though electromagnetic coupling. Most lightning strikes are of negative polarity and thus the induced voltages are positive. According to [5] the number of induced surges exceeding 100 kV, on an unshielded 9 m high line, is approximately the same as the number of direct strikes. Induced voltages have a maximum of 250 kV but rarely exceed 200 kV [5]. The selection of a structural BIL of 300 kV includes compensation for wet conditions. If the lightning strike is beyond a distance of 300 m the induced effects may be disregarded [6].

The rise time of the induced waveform from the first stroke is typically 5 to 10 μs. The return stroke velocity affects the induced voltage waveform's magnitude, front time and decay time. As the velocity of the return stroke increases, the amplitude of the induced voltage decreases, the induced voltage front steepness increases and the amplitude is proportional to the return stroke current. Variation in the time to half value of the return stroke current has negligible effect on the induced voltage waveform. The closer the stroke is to the distribution line the larger the induced effects. Generally, as the ground conductivity decreases, the induced voltage amplitude increases [7]. The basic insulation level (BIL) of the line equipment is specified in terms of the 1.2/50 μs test waveform, but induced voltages usually have slower rise times and quicker decay times, thus the induced waveforms

will stress the line insulation less than expected.

Since indirect strikes induce voltages with maximum voltage of 250 kV and the BIL of the line is 300 kV, it is unlikely that an indirect lightning strike will cause flash-over. Direct strokes have a much higher magnitude and will thus be the focus of the simulations. Future investigations may include the effects of induced strokes.

C. Source

The investigation is of a 22 kV distribution system, thus an appropriate source is required for the simulation. A Type 14, steady-state continuous 50 Hz source was used. A source impedance was required, for this purpose a 0.5 Ω reactance was added per phase. This arrangement proved to be adequate for the purposes of the investigation.

D. Pole Configuration

In South Africa, wood poles are commonly used for distribution lines. In sparsely populated rural areas there are longer spans of line and fewer transformers therefore fewer surge arrestors. In this scenario wood poles provide a higher BIL and a better lightning performance. Due to the arc quenching properties of wood it is possible to avoid power arc follow-through by using a length of wood in series with the insulator hardware and an earthed down-lead. The effectiveness of this setup depends predominantly on the lightning impulse strength of the wood which is directly related to the wood gap length and the moisture content. Secondary influences on the arc quenching properties of wood are the cross-section, species, degree of creosoting, and weather conditions [8] & [9].

In areas of low lightning activity, wood or concrete poles with no down-wire on the wood poles may be used. Low lightning activity is defined to be less than 4 ground flashes per square kilometre per year; in most high-veld areas this number is easily exceeded. In areas of high lightning activity, wood poles are used with a BIL of 300 kV. The 300 kV BIL is achieved by taking into account the flashover voltage of the insulator (on each phase) and then by installing a down-wire with a spark gap of 500 mm between the down-wire and the MV insulator closest to the ground [2].

Due to the large currents injected by direct strikes and the arc quenching properties of wood, there is a possibility that the wooden cross-arms and poles can sustain mechanical damage.

The wood needs to be seasoned since the moisture content is an important factor in determining the strength. As moisture content increases, the resistance of the wood decreases. The moisture content is a determining factor of the breakdown path (i.e. if it is external or internal). If breakdown occurs internally there is a very high probability of shattering. The length of wood between the insulators and the down conductor is very important in determining whether the

discharge path is internal or external. If the gap is longer than 600 mm (even for seasoned wood) then the discharge path is likely to be internal [8]. To avoid damage, but allowing current to flow on the wood surface, a metal band or strap may be used. This method is useful especially if the wood pole has not been seasoned long enough and is still wet. When the pole is wet due to rain, the current flows along the pole surface and damage is not incurred. If the length of wood is longer, the BIL increases and the severity of surges transferred to equipment increases; thus there is an increase in arrestor operation. It has been found that Eucalyptus cloeziana is the best type of wood to be used since it has a high mechanical strength and is more resistant to shattering under high current discharge conditions [8] & [9].

When designing (or modelling) a distribution line it is important to consider that the dry impulse strength decreases by an average of approximately 40% in wet conditions [5]. Negligible improvement of induced surge performance will be achieved by increasing the dry BIL of the line above 350 kV. It would be advantageous to rather seek the weak line structures (where "weak" is defined by the conditions and specifications of the design) in the system and compensate for this weakness. One "weak" point in the system may drastically effect the performance of the line.

Most of the distribution lines in rural South African areas have a triangular phase structure with the centre phase raised in order to reduce the risk of electrocuting birds. See Figure 1. The second design commonly used is the staggered vertical configuration shown in Figure 2. The triangular phase structure was used in simulations since it is the easiest configuration with which to achieve a 300 kV BIL, and the most symmetrical in terms of electrical modelling. Figure 3 shows the electrical configuration of the pole, the letters A, B, and C represent the phase connections, while the resistances R_A, R_B and R_C represent the arcing paths, essentially between the phases, to the common point from which the final arcing path to ground is represented by R_{flash}. Figure 4 shows an approximate electrical model for the staggered vertical configuration, this configuration is more difficult to work with since the achievement of a 300 kV BIL is non-trivial. The footing resistance of the pole is R_{gnd} while the inductance of the down-wire is L_{gnd}. The inductance is calculated as approximately 1 μH per m of cable, and is estimated as 7 μH per pole. The footing resistance was estimated by considering the distribution line without surge arrestors, applying the 35 kA lightning impulse, and altering the footing resistance until flash-over occurred for approximately 6 poles either side of the strike location. The ground resistivity of the region where the measurements were take is in the region of 1000 $\Omega.m$. The pole earthing is in the form of the earth wire being wrapped around the planting section of the pole - commonly termed a 'butt-wrap'. The resistance of the pole footing, used in the model of the pole, was taken to be approximately 150 Ω. The switch shown is a voltage controlled switch, i.e. upon detecting a potential in excess of 300 kV the switch closes

for a minimum period of time of 10 μs or until the current reaches a defined lower limit. It would be more precise to use two, or more, switches in series. The first switch would model the flashover of the insulator while the second switch would represent the flashover of the wooden gap. Flashover across the first set of resistors (R_A, R_B and R_C in Figure 3) may not be directly in contact with the wood surface since the flash-over of the insulator may go directly to the steel support, this would leave the last gap, R_{flash}, as the main flashover path. The arc represented by R_{flash} would be over the wood surface. This would result in a simplification to the triangular pole model's electrical model configuration. Thus the resistances R_A, R_B and R_C in Figure 3 become short-circuited.
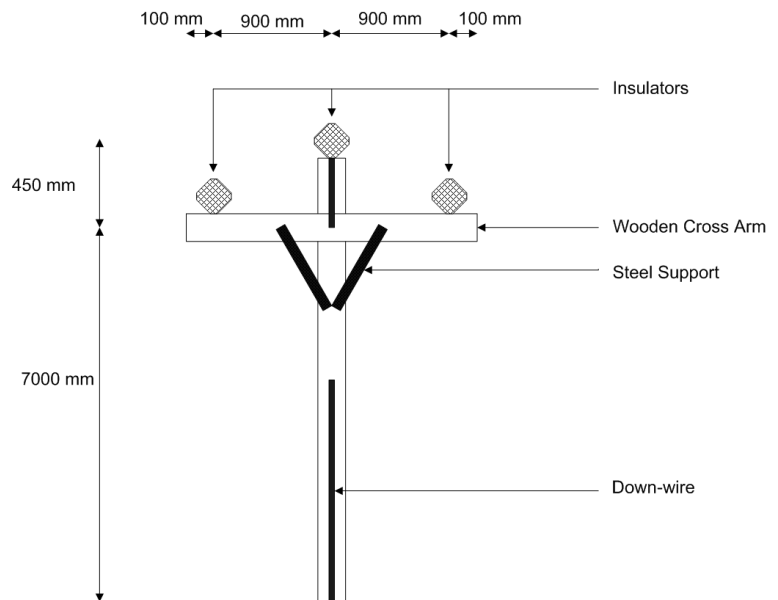

Fig. 1.   Triangular pole configuration

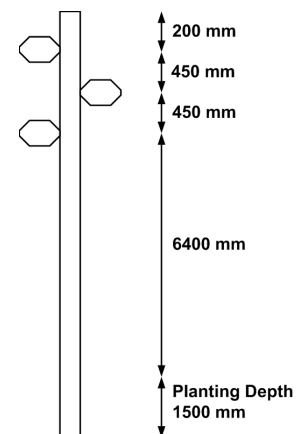Fig. 2.   Staggered vertical (zero degree deviation) pole cofiguration

E. Line and Spanning Model

The line model used was the J. Marti frequency dependent model. This model is sufficiently accurate for simulation
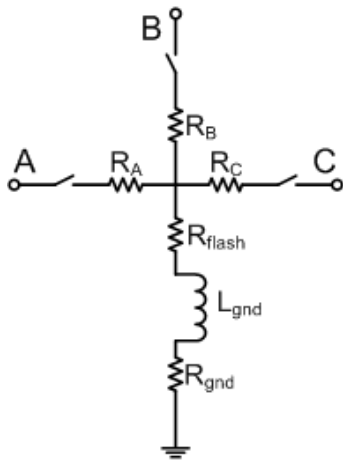
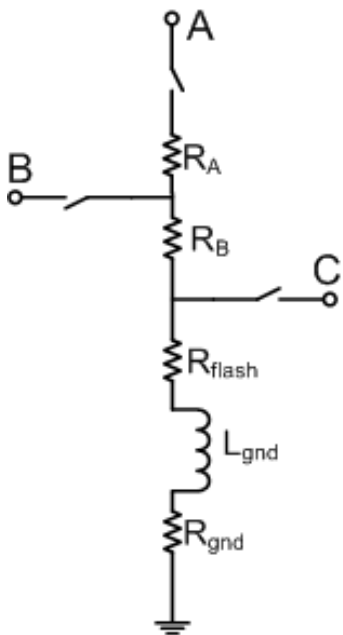Fig. 3.   Electrical model for trinagular configuration

Fig. 4.   Electrical model for staggered vertical configuration

purposes. The distribution line model was constructed with 150 m segments (or spans) since the arc quenching model to be introduced is part of each pole. A total of twenty four spans were used and to avoid complications in terms of reflections a 5 km segment of line was added to both the beginning and end sections of the line. The J. Marti settings were that of a 3 phase overhead line, with 8 decades and 10 points per decade. A steady state frequency of 50 Hz and frequency matrix of 500 kHz, default filtering was implemented. The ground resistivity was taken to be 1000 $\Omega.m$ and the lower frequency as 0.005 Hz. The type of cable used was fox with current rating of 155 A, diameter of 8.37 mm, and DC resistance of 0.7822 Ω/km.

F. Surge Arrestors

Equipment installed on 22 kV networks typically has a BIL of 150 kV, which is much lower than the 300 kV BIL of the line. Direct, and some indirect strikes, will

exceed the equipment BIL; therefore surge arrestors are required [2]. Direct strikes pose the largest hazard to surge arrestors due to fast wave-fronts and large current magnitudes.

There are two main types of surge arrestors, namely gapped and gapless. Gapless arrestors are most common and will be the only type of arrestors to be considered in this investigation. Surge arrestors act as a high impedance during normal operating conditions. As soon as a voltage exceeds the arrestor clamping voltage the arrestor behaves as a low impedance, thereby conducting surge current to ground and limiting the voltage developed across the equipment being protected. The voltage developed across the equipment is the sum of the voltdrop across the arrestor terminals and the inductive voltage developed (by the surge current) in the arrestor line and ground leads [10].

To limit the inductive voltdrop, surge arrestors should be installed as close as possible to sensitive equipment and have short leads. These inductive voltages coupled with the arrestor voltdrop may exceed the BIL of the equipment being protected. The rate of rise associated with the lightning waveform is important when considering inductive voltdrops.

Most distribution circuits will also undergo numerous changes as arrestors will fail, insulators are replaced, circuit sections are switched in and out, and, rarely, poles need to be replaced. To reduce flashovers due to direct strikes the number of arrestors may be increased (shorter spacing between arrestors). As the number of arrestors increases so does the probability of arrestor failure [11]. If arrestors fail then the consequences may be costly since the line may be in a state of no or little protection. Arrestors may also fail in the event of a long duration lightning stroke, although these are rare.

An arrestor current rating of 10 kA is used in most applications. If the lightning current has a high probability of exceeding the arrestor rating (rare) fuses may need to be installed. Arrestors selected need to have a sufficiently high maximum continuous operating voltage (MCOV) to prevent thermal run-away caused by normal operating voltages and temporary over-voltages.

In South Africa, at a transformer installation, arrestors are normally mounted on all three phases of the line. In rural areas with low population densities the spacing of transformers is in the region of 1 to 5 km [8] & [12]. In densely populated areas transformers are placed, on average, every 100 or 200 m [8]. For this study the measurements were taken on a rural distribution line, thus placement of arrestors was selected to be approximately every 1 km.

In densely populated, suburban, areas there are on average more trees and buildings thus reducing the number of direct strikes but increasing the number of indirect strikes (not generally proportionally).

Arrestors on the pole (or phase) which is struck directly will be subjected to most of the initial current in the rise period of the injected current waveform. By placing arrestors on adjacent poles, significant amounts of current from the tail of the stroke waveform will be shared. This effect reduces the tail time constant of the struck arrestor's discharge current. By reducing the current, the energy is also reduced [8].

Shield wires may be used to reduce over-voltages, but are financially unviable in the case of distribution lines. The proposed cost of installing a shield wire is estimated by [8] to be R7000 per km. The advantages of installing a shield wire are briefly discussed for completeness. It is estimated that surge arrestors installed on a line without overhead shield wires must deal with increased energy absorption 3 to 5 times greater than those installed on a line with shielding. It is more effective to install a shield wire than to increase the arrestor rating by two-fold [11]. Shield wires often require surge arrestors to prevent back-flash-over, but the energy dissipated by the arrestors is lower than that of arrestors on an unshielded line. The footing resistance of the poles is an important factor to be considered when installing surge arrestors.

If weak points (e.g. poles with unacceptable footing resistance) can be easily identified then surge arrestors may be installed to add extra benefit in terms of reducing the number of flash-overs.

For areas of extremely high lightning activity, specifically high current lightning, it is possible to use sets of arrestors in parallel. The effect is that the energy absorption of a single arrestor is greatly reduced; the downfall is that the arrestors need to have almost the same discharge voltages and voltage-current characteristics [13].

The modelling of surge arrestors is a complex procedure due to the non-linear properties of these devices. A model developed by the IEEE Working Group 3.4.11 [14] was considered but this model relies on many measured parameters which are difficult to obtain from manufacturer data-sheets. Pinceti [15] developed a simplified version of the IEEE model without loss of accuracy. Figure 5 A shows the Pinceti model. The values of resistance is chosen to be 1 MΩ for stability of the calculation while the inductances and non-linear elements are specified in terms of a combination of data-sheet information and calculations developed by the IEEE Working Group 3.4.11.

Though simulation it was found that a complicated model was prone to introduce errors into the calculations, and in certain cases unexplained oscillations. A simplistic model proved to be the most accurate, and was sufficient for the investigation. This simpler model consisted of a single non-linear element (shown in 5 B). The non-linear characteristic was modelled on data from the ABB POLIM-S20N [16] and techniques adapted from the IEEE and Pinceti models. The model used proved to be sufficiently accurate for the purposes of the investigation.
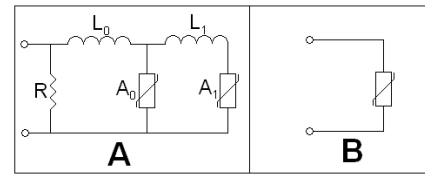

Fig. 5.   Pinceti Surge Arrestor Circuit Model

Figure 6 shows the Voltage-time (V-t) curve of the load being protected by the implemented surge arrestor model. This surge arrestor was placed 450 m along the line from the pole which was struck by lightning. The phase on which the measurement took place is that of the strike. The lightning source used was the same as that described in section II-A. Further discussion
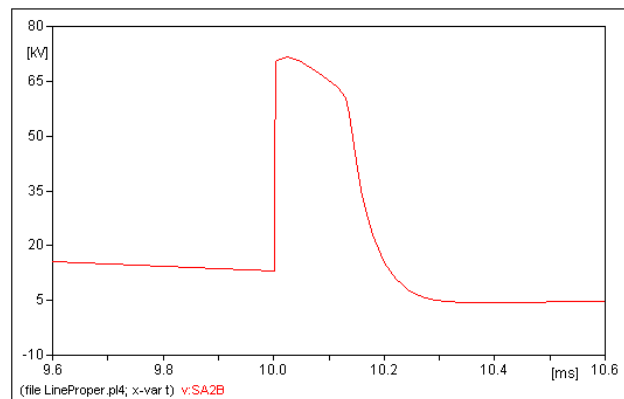

Fig. 6.   Simulation V-t curve of Surge Arrestor 450 m from strike location

regarding surge arrestor modeling is available in [14] and [15].

G. Termination and Transformers

The correct modelling of line termination and the transformers on the branch sections is important in terms of achieving the correct frequency response of the line. If the line is terminated in a pure resistance there is significant attenuation and in some cases (especially when the resistance is approximately matched to the line impedance) resonance. Distribution lines are usually terminated with a transformer, which on the most basic level can be modelled as a capacitance. A more accurate model was found in [17] and is shown in Figure 7. This model is based on results form voltage impulse tests.

H. Initial Simulation Results

The simulation results may not be an accurate reflection of the distribution line on which the measurements were taken, since the exact specifications of the line are unknown. For instance, there could be more than one type of distribution line pole configuration used at crossing sections and where transformers are located, or the type of conductor may be different, and most likely would be that the network consists of various interconnections and mesh branches.
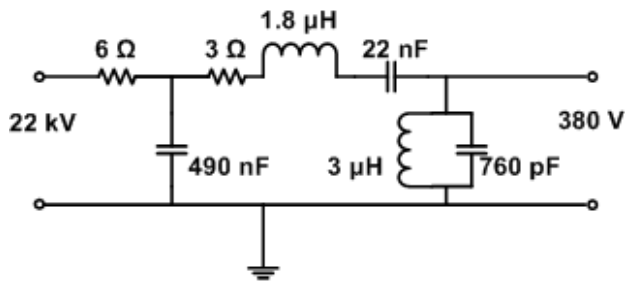
Fig. 7.   Electrical model of a 22 kV/380 V 100 kVA distribution transformer

Fig. 9.   High level model of simulation distribution line model

The modelling of branch-off sections and transformers was not considered in detail, transformer models were protected by surge arrestors. The initial simulations included a very simplistic static resistive arc model.

The field measurement from Eskom is shown in Figure 8. The overvoltage is lower than 2 p.u. (per unit), and the line stabilises in approximately 10 ms (from the initiation of the overvoltage condition). The exact position, on the distribution line, of these measurements is unknown, but since there seems to be little indication of surge arrestor action it is likely that the measurement was taken far from the point of strike. It seems likely that the measurement was conducted on a parallel branch of the main line. To take this possibility into account parallel lines needed to be added to the distribution line model. The parallel lines were simplistic, and only consisted of J. Marti models, not including surge arrestor or pole models.
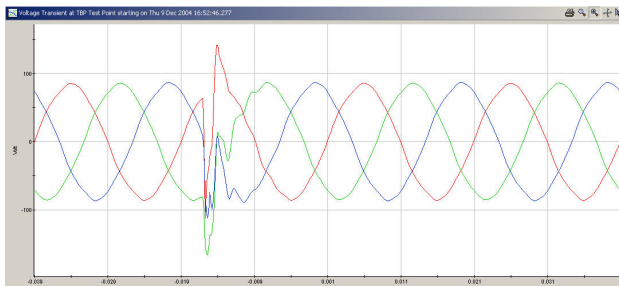
Fig. 8.   Eskom field distribution line measurement

The simulation results were taken at various locations on the line, specifically at the beginning, 5 km from the termination, at the termination, and selected points on the parallel lines. The lightning current source was placed in the centre of the main distribution line (attached to a single phase), and had a magnitude of 35 kA. Two configurations were tested for the transformer secondary; open circuit and loaded with 3300 Ω. It was found that there was very little difference between loaded and unloaded conditions for all the simulation measurement positions.

Figure 9 shows a flow diagram of the line configuration. The first set of simulations was for a distribution line which had loaded transformers and surge arrestors. The voltage waveform shown in Figure 10 is from the beginning of the line (generation side); directly after the 5 km segment. The
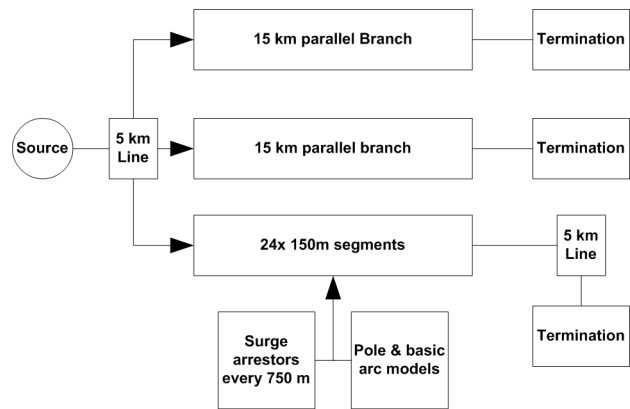
action of the surge protection is visible around the 10 ms mark, and the phase voltages recover from the transient after 7 ms. Figure 11 is at the end (termination side) of the main distribution line just before the final 5 km line segment, it is very similar to that shown in Figure 10. This result is not unexpected since the distribution line is symmetrical between the defined begin and end points. The third measurement, (Figure 12), is from the very end of the main distribution line, after the last 5 km segment. Since a surge arrestor is protecting the termination load the voltage clamping just after 10 ms is expected. The voltage also takes a longer time to stabilise.

On the first 15 km parallel segment three measurements were taken (every five kilometres). While on the second line, also 15 km in length, the measurement was taken at the end of the line. Figure 13 and Figure 14 show significant resonance following the 10 ms time marking, but the measurement from the end of the line (Figure 15) shows very little resonance and little arrestor action. It was expected that the simulation measurements at both parallel branch ends would be similar. This was the case and thus only one of the branch end measurements is shown.

For comparison, the two of the simulation results for the scenario of no surge protection are shown in Figures 16 and 17. The first of the two figures is the voltage waveform at the beginning of the line, and the second is the voltage waveform at the termination of a parallel branch. The full complement of results is included in Appendix I.

The voltage measurements are not sufficient to evaluate the effects of the static arc model. Therefore it is necessary to include the current distribution along the distribution line and down the poles to the arc models, from the point of lightning strike. The set of simulation data presented consists of three figures (18, 19, and 20) which are the current travelling towards the source (left), towards the line termination (right), and to the nearest arc (down). The directional abbreviations of left, right and down will retain their meaning for the remainder of the paper. The current distribution along the line is high (15 kA) while the current through the static arc model is approximately half this value. At this point these measurements have little meaning, but are important for
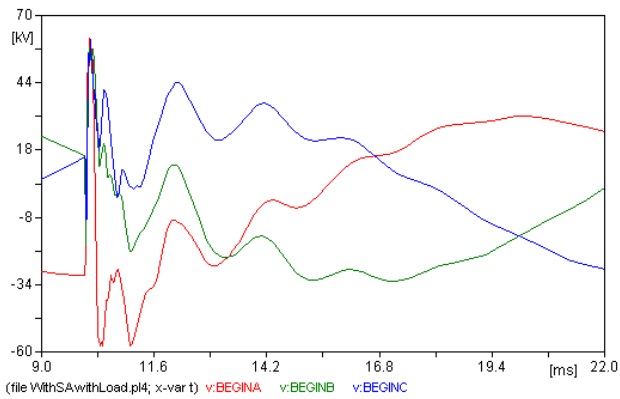
Fig. 10.   Simulation voltage measurement from the beginning of the line
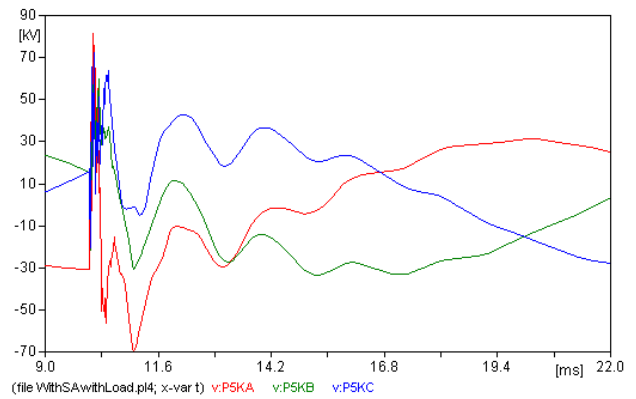

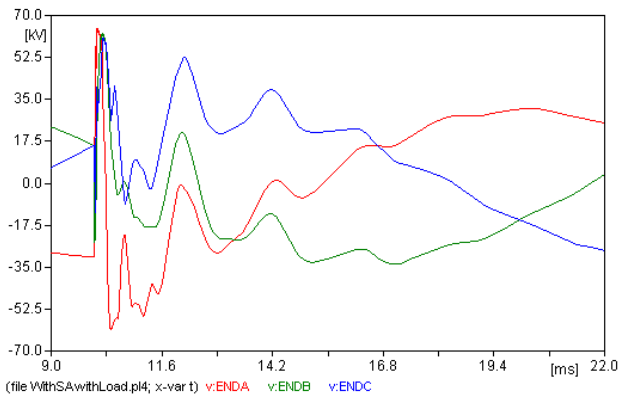Fig. 13.   Simulation measurement after 5 km of the first parallel branch

Fig. 11.   Simulation voltage measurement from the end of the line
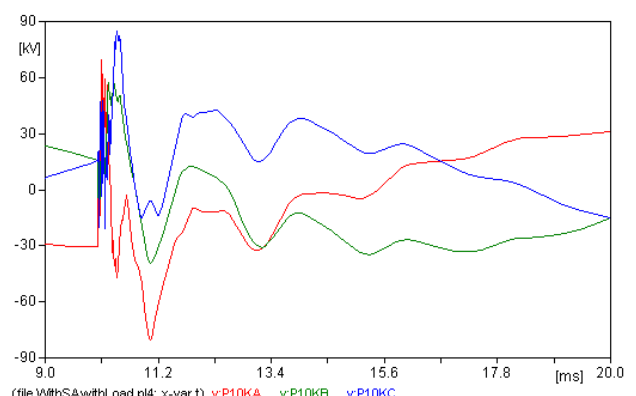

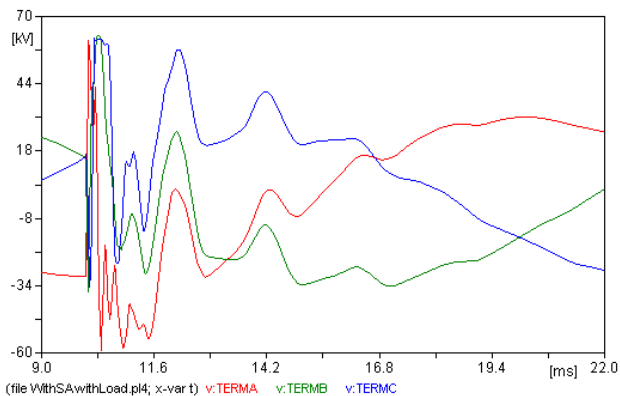Fig. 14.   Simulation measurement after 10 km of the first parallel branch

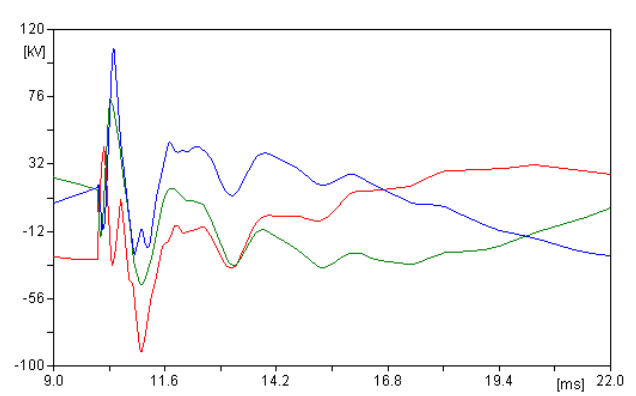Fig. 12.   Simulation measurement from the termination of the line

Fig. 15.   Simulation measurement from the termination of the parallel branch

evaluation of the dynamic arc model. The current distribution through the static arc models on five poles to the left and right of the point of strike is presented in Appendix I. A more comprehensive discussion of the results obtained from these initial simulations follows in section V alongside a discussion of the full arc model.

III.   ARC MODELING

The electric arc is a complex phenomenon. The first part of this section is dedicated to developing an understanding of the arc process by providing some general background and then discussing, specifically, the AC arc. Arc formation and extinguishing, which falls under the topic of plasma physics, is a complicated topic and there is a large quantity of literature which attempts to describe various aspects. This section provides a summary of some selected topics which are directly related to the investigation at hand. The second part of this section discusses aspects of the mathematical modelling of an AC arc, followed by an attempt to implement the relevant combination of equations in an ATP-EMTP simulation. Much of the research relating to the arc phenomena discussed in this investigation has been done in order to advance understanding
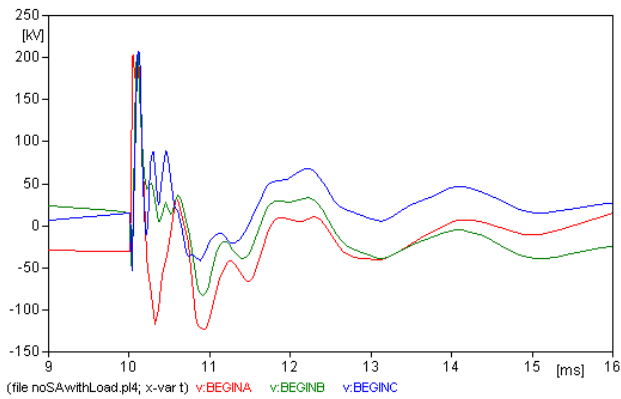
Fig. 16. Simulation voltage measurement at the beginning of the struck distribution line
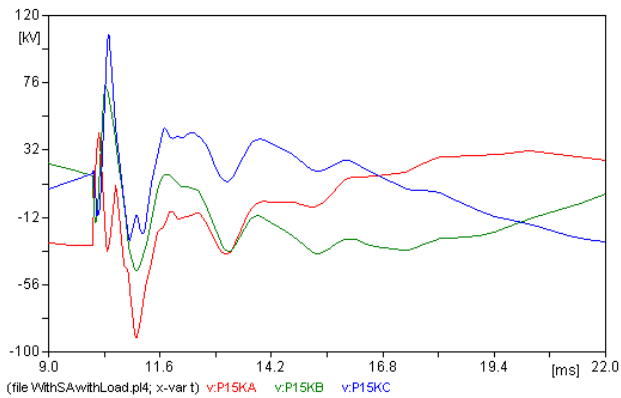
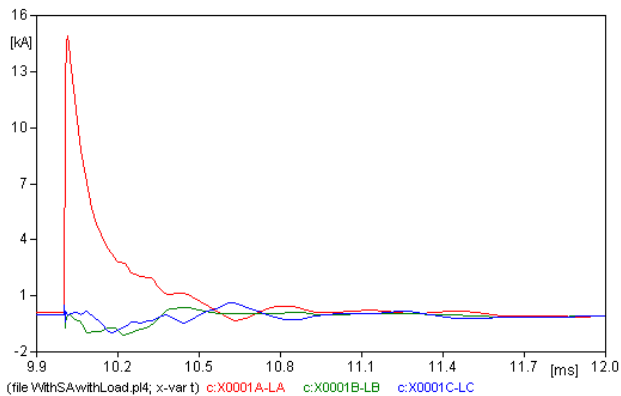Fig. 17. Simulation voltage measurement from the termination of the parallel branch

Fig. 18. Current component travelling left of the point of strike - static arc model
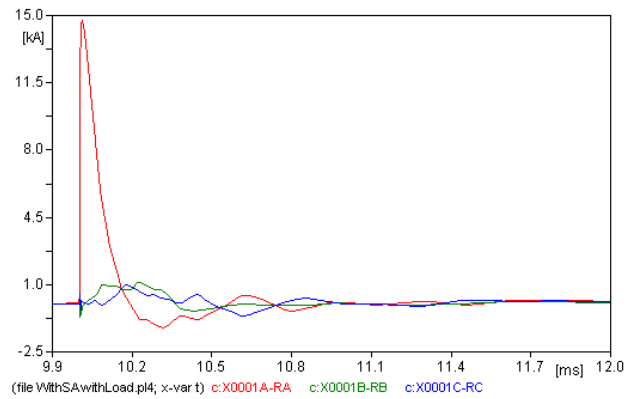

Fig. 19. Current component travelling right of the point of strike - static arc model
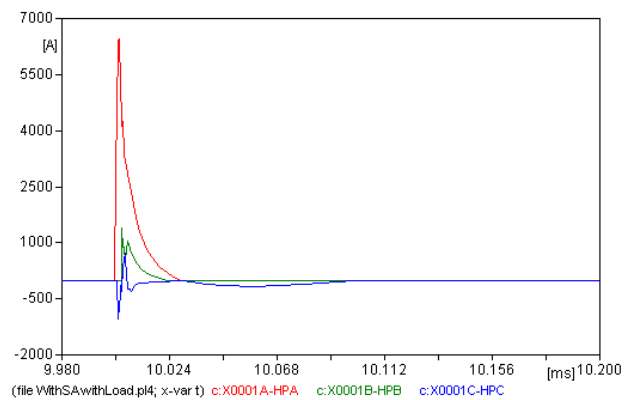
Fig. 20. Current component travelling through the arc closest the point of strike - static arc model

of circuit breaking techniques and improve equipment in use. Therefore it is necessary to examine equations and methods of implementation carefully since there are subtle differences between circuit breakers and the arc model under investigation.

A. The Arc Process

1) General Background: The glow and arc discharge are both types of current sustained plasmas. Glow is the initial discharge which precedes the arc. The arc is characterised by a small, yet intensely bright core surrounded by the aureole (region of flaming gas). The centre of the arc column consists of dissociated gas. The transition from glow to arc occurs when the cathode becomes completely covered in glow, the discharge current increases, the current density at the cathode increases and an abnormal glow forms. A critical value of voltage is reached, and provided that the power source is capable of supplying (and maintaining) high currents, an arc forms across the gap. After the transition the current density becomes almost independent of the arc current since the electron emission of the arc is very different to that of the glow [18]. The pressure of the surrounding gas also influences the transition from glow to arc. An increasing current flow through the arc leads to a voltage drop across the arc, thus the slope of the V-I characteristic is negative. If the currents are very high (i.e. 10 kA) then the slope may be positive [18]. Literature refers to the high pressure and low pressure conditions. High pressure is defined as a pressure greater than 200 mm Hg, where the gas temperature is approximately the same as the electron temperature. At lower pressures ($<$ 200 mm Hg) the gas temperature and the electron temperature curves diverge. Since the investigation is for approximate atmospheric conditions (760 mm Hg) the arc operates in the high pressure region.

Due to the high temperatures created by the large currents flowing through the arc, the surrounding medium (usually gas) is heated and a convection system is established, thus the arc shifts position continuously. Through this movement the column arches (thus the name electric arc came into existence) and the actual length of the column changes for a constant electrode spacing. For vertical electrodes the hot gasses rise and may change the phenomena of electrode particle loss of the upper electrode. For long arcs (500 mm is considered long) a spectrum of electrode vapour is usually only found near the electrodes and not in the gap [18]. At atmospheric pressure the charged particle density near the centre of the arc column ranges from 10^{14} to 10^{18} $electrons/cm^3$ ([19] & [20]). The quantity of impurities (including oxides) on a metal electrode surface affects the current density (a large quantity of impurities will increase the current density).

There are three main types of arc classified according to the mechanism used to achieve electron emission from the cathode:

1) Thermionic arc with the cathode heated by an external source
2) Thermionic arc where the arc heats the cathode
3) Field-emission arc. A large electric field is produced by space charge of positive ions a short distance from the cathode or by a very thin layer of insulating material with its surface raised in potential by the accumulation of positive ions (The Malter-Paltow effect). Electrons are emitted from the cathode by the action of the electric field.

Method 1 is not self sustaining, while methods 2 & 3 are self sustaining. Liquid metal electrodes follow different principles and are not discussed in this paper.

If the arc length is increased then the voltage required is higher, the interesting point is that the increase in voltage is almost linear. The cathode and anode voltages (rise or drop) usually remain constant independent of the change in arc length [19]. The temperature in the arc column approaches 4000 K for pressure of 1 atmosphere. The arc is distinguished from other electrical phenomena as it is a discharge in a gas medium which is approximately in thermal equilibrium. Certain factors aid in the establishment of the equilibrium; short mean free path, field strength and high temperature. Since an approximate thermal equilibrium is established it is possible to apply thermodynamic laws (even though the individual processes leading to the final state may not be known) [21]. Thus the thermodynamic Saha equation may be used to calculate the density of charged particles in the column as a function of temperature and pressure [19].

The type of surface that the arc travels above, or over, influences the properties of the arc. Darveniza [22] discusses four categories of surface:

1) Smooth surface in a uniform field. Generally glass or porcelain. Results in a reduced flashover voltage, compared to air. Generally by a factor of 0.3 for gaps 10's of cm. A decrease in pressure results in a decrease in the flash-over voltage, but the rate of decrease with regard to pressure is slower for a solid surface than for air. Other factors are; air humidity, surface roughness, dust, surface charge, and non-uniform leakage currents.
2) Smooth surface in non-uniform field. A non-uniform field has components in both tangential and normal to the insulating surface. There is a dependence on the breakdown voltage on the relative permittivity of the solid since some of the field lines pass through the dielectric. As the permittivity approaches unity the breakdown voltage increases.
3) Corrugated surfaces. Sometimes the arc passes over the surface and other times through air. The corrugation increases the flash-over voltage. This type of surface is important in the design of bushings and insulators, but not applicable to the research topic of this paper.
4) Contamination. Contamination is most commonly found as pollution. The effect of deposits is a reduction in flashover voltage. Contamination will not be considered in the modeling of the arc across a wood surface.

The wooden surface of distribution line poles would be classified as a smooth surface in a non-uniform field. Depending on the quality and type of wood it is possible to overlap with the corrugated surface. Contaminated surfaces are not considered within the scope of this research and the formation of an arc has a different 'breakdown' process.

2) The AC Arc: The voltage across the arc may be characterised by the reignition voltage, burning voltage (approximately constant), and the extinguishing voltage. In the case of an AC arc if the steady state power frequency is lower than 100 Hz then the characteristics of the arc are approximately the same as that of a constant voltage. Every time that a current zero is reached the arc extinguishes, but the ionized particles in the column take a finite amount of time to recombine or diffuse from the arc plasma channel. New ionized particles are not created in the current zero period. If sufficient particles remain in the channel then the restrike voltage required is lower. If restrike occurs then the voltage drops and the current rises. The restrike period is also a function of the gap and electrode geometry [19]. Compared to the case of a static voltage supply, due to the period of cooling (current zero) the burning voltage during the current rising period is greater than that for the static case. While after a current maximum the ionization process is at a maximum and as the current decreases the burning voltage is lower than the static case. For metal electrodes the extinguishing voltage is high since glow discharge often occurs before a current zero.

Presuming an arc has been established, if the system passes through a power frequency current zero and the current flow is not re-established, a voltage (restriking voltage) appears between the electrodes. Most power system circuits have a certain amount of inductance, thus the current and voltage waveforms are not in phase. This leads to the recovery voltage approaching its peak when the current is near

a 'natural' zero. This condition aids in the restriking of the arc [23]. If the voltage and current are approximately in phase then the arc will most likely be extinguished permanently. In the inductive circuit the distributed capacitance of the circuit is charged when the applied voltage is at a maximum and current is zero, thus the recovery voltage can reach its peak at twice the voltage of the supply. Recovery strength is a better term to describe the strength of the arc gap. Many texts refer to the dielectric recovery voltage, but this is technically not correct since the material in the gap is dissociated and ionized therefore the term dielectric does not apply. After arc extinguishing there is a rapid increase in the recovery strength of the gap, the area surrounding the electrodes soon form layers of neutral gas due to deionization of ionized particles. The rate of recovery strength slows after this initial burst since the column maintains a high temperature and becomes slightly isolated from the electrodes [18]. A reduction in the gas density of the column would decrease the breakdown voltage of the gap even if no ionized particles were present. As the recovery voltage increases energy is injected into the column though electron collision ionization. Depending on the rise of recovery voltage and the ionization effect of the E-field the arc may be re-established.

Consider an explanation of the restrike phenomena through a theoretical example. An arc which has a finite conductance at a current zero and no further energy input, and has a finite conductance decay time. Due to the conductance being non-zero there is a post arc current flow which alters the restrike voltage. Therefore the resulting power flow will determine if there is a decay in the conductance, and if the arc extinguishes or if there is thermal re-ignition [23].

In the case of no thermal re-ignition, the discharge current will decay to zero and the restrike voltage rises. Depending on the temperature and density of the arc column gas the voltage required to breakdown the gap may be small (Recovery voltage). If the recovery voltage equals or falls below the voltage across the gap then the will be restriking of the arc. If the restrike voltage exceeds the voltage over the gap then there is no breakdown.

A more practical example follows: For a resistive circuit consider Figure 21 adapted from Cobine [18]. At point A
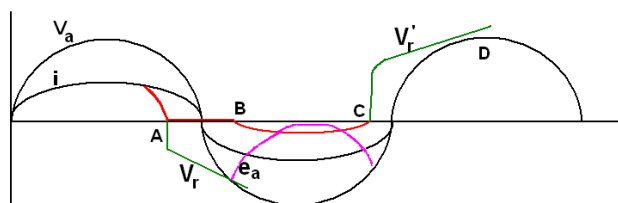
Fig. 21. Arc phenomena of a resistive circuit

the arc current reduces and the arc voltage increases (e_a). Shortly after, the arc extinguishes the recovery strength of the gap increases. The reignition voltage rises and at point B the reignition voltage is equal to the circuit voltage and the arc reignites. At point C the process repeats but the

recovery strength may be higher than at point A due to a reduced current flow. Thus the reignition voltage (at point D) is too high for the circuit voltage to reach and the arc is extinguished permanently.

As mentioned above in the case of an inductive circuit the voltage and current are out of phase and together with the circuit's distributed capacitance thus lowering the time allowed for recovery. If the circuit happened to be capacitive then the conditions for extinguishing the arc are favourable since for zero current the applied voltage is rising very slowly. In the case of circuit breakers it is possible to install a shunt resistance across the arc gap which would limit the rate of rise of the recovery voltage to less than the rate of recovery strength (which varies inversely to the current) [18].

The arc performs power factor correction (for an inductive circuit). This can be seen by considering a voltage source in series with the circuit inductance, resistance and the arc. The resistance is often small in comparison to the inductance, thus may be ignored without introducing significant error. By integrating the system's first order differential equation over a period 0 to t, and by making the current (i) the subject Equation 1 is found.

$$i = -\frac{V_m}{\omega L}cos(\omega t + \phi) + \frac{V_m}{\omega L}cos(\phi) - \frac{e_a}{\omega L}\omega t \qquad (1)$$

Where:

i	= Instantaneous value of current
V_m	= Peak supply voltage
L	= Circuit inductance
$\omega = 2\pi f$	= Supply frequency
ϕ	= Angle measured from instant of zero current
e_a	= Arc voltage

If $\omega t = \pi$ and the current is zero then the magnitude and phase equations are shown in Equation 2.

$$-V_m(cos(\pi + \phi) - cos(\phi) = e_a \pi \phi = cos^{-1}(\frac{\pi e_a}{2V_m}) \quad (2)$$

There is a 'capacitive' shift due to the dissipation of energy in the arc. Therefore the ratio of arc voltage to applied voltage increases and the angle between applied voltage and current is smaller. For example if $\frac{V_m}{4}$ = arc voltage then the phase shift will be $\phi \approx 67°$ instead of $\phi \approx 90°$ [18].

B. Dynamic Arc Models

Most mathematical arc models are analytically complex and formidable to solve. Differential equation type models are based on the energy balance equation developed by Weizel and Rompe, shown by equation 3.

$$E.j - i + div(K).grad(T) - d.C_p.\frac{dT}{dt} - eV_i\frac{dn}{dt} \qquad (3)$$

$$= eV_i.div(D_{am}).grad(n)$$

Where:

$E.j$ = Joule heat supplied
i = Energy loss due to light emission
$d.C_p.\frac{dT}{dt}$ = Energy loss due to gas heating
$eV_i\frac{dn}{dt}$ = Energy loss due to ionization

The term $eV_i.div(D_{am}).grad(n)$ represents the energy gained by the system due to the current flowing through the arc.

Two types of mathematical model were attempted for the modeling of the arcing process. The first is based on both the Cassie and Mayr models and describes the entire arcing process while the second model is less accurate and based only on a form of the Mayr model. Each of these models is discussed in detail below. A very comprehensive summary of the various arc models available is presented in [24].

1) Model 1: This model consists of two distinct segments. The first segment consists of the Cassie differential equation which was proposed by Cassie in 1939, the derivation is discussed in [23]. To obtain the Cassie equation from the thermodynamic energy balance equation the following assumptions (simplifications) are necessary:

- The arc column is cylindrical, has a well defined boundary and uniform temperature distribution over its cross-section. In other words within the boundary there is a finite resistivity and constant energy distribution per unit volume
- Temperature remains constant as the cross-sectional area adjusts itself to accommodate the changes in current injected by the external circuit.
- Power dissipated is proportional to the column cross-section.

The Cassie arc model differential equation is shown in equation 4.

$$\frac{dG_c}{dt} = \frac{1}{\tau_c}\left(\frac{i_a^2}{U_c^2.G_c} - G_c\right) \quad (4)$$

Where:

G_c = Cassie arc conductance
τ_c = Cassie time constant of the arc
i_a = Current
U_c = Steady state arc voltage

The downfall of the Cassie equation is that it is not capable of describing the arcing process in regions of a current zero, or describing the formation of the recovery voltage.

The Mayr model presented by Mayr in 1943 was designed for use in the region of a power system current zero, i.e. for current in the region of tens of amperes. For higher currents the differential equation (D.E.) will still converge to a solution but is not as accurate as those presented by the Cassie D.E. Thermal conduction was considered as the dominant mechanism for energy removal. Some of the assumptions necessary to obtain the Mayr equation from equation 3 are:

- The cross section of the column is assumed constant.

- The conductivity is assumed to vary as a function of temperature in order to compensate for the injected current.

The Mayr equation is presented as equation 5

$$\frac{dG_m}{dt} = \frac{1}{\tau_m}\left(\frac{i_a^2}{P_0} - G_m\right) \quad (5)$$

Where:

G_m = Mayr arc conductance
τ_m = Mayr time constant of the arc
i_a = Current
P_0 = Steady state power loss of the arc

Since the Cassie arc model describes the arc in a region of high current and the Mayr equation is more accurate for regions of low current it would be beneficial to combine these two models to describe the entire arc process accurately. Various methods to combine the two equation have been found in literature (such as the methods presented by Frost [25] and Browne [26]) but the most interesting is that presented by Habedank [27]. The Habedank model is simplistic and works exclusively with parallel conductances, shown by equation 6.

$$\frac{1}{G_T} = \frac{1}{G_m} + \frac{1}{G_c} \quad (6)$$

Where:

G_T = Total arc conductance
G_m = Mayr arc conductance
G_c = Cassie arc conductance

In the Habedank model when the currents are high almost all the voltage drop is over the Cassie part, but before a current zero the Mayr contribution increases and represents all the recovery voltage as the Cassie portion approaches zero. From equations 4 and 5 there are a total of four parameters. The parameters are:

τ_c = Cassie time constant of the arc
τ_m = Mayr time constant of the arc
U_c = Constant part of the arc voltage
P_0 = Steady state power loss of the arc

These parameters describe the arcing process. For the modelling of the arc over a wood surface these parameters require further investigation. The time constants are dependent on the arc length, which is one of the most influential factors on the self-extinguishing properties of the arc. The time constant defines the rate of arc conductance change. The time constants are also dependent on the energy content and thermal power dissipation of the arc. The Cassie time constant is expected to be in the region of 1 μs and the Mayr time constant in the region of 0.1 to 0.2 μs [27]. The parameters P_0 and U_c describe the rate of energy removal.

The problem with the Habedank model, or combinations of Cassie and Mayr models, is that the computer simulations are conducted in parallel with experiments and thus many of the variables and parameters may be solved from measured

data. A more in depth study of the system reveals that the Mayr DE is trivial to solve and the solution is obtainable by using ATP-EMTP. The Cassie D.E. is not variable separable and cannot be written in the form shown by equation 7, thus cannot be solved by ATP-EMTP. To find the solution one method would be to use an application such as Matlab [28] but this would require that ATP-EMTP and Matlab are interfaced during the simulation.

$$(a_0 + a_1 D + a_2 D^2 + \ldots + a_n D^n)y = x \qquad (7)$$

Where:

D = Differential time operator (d/dt)
y = Variable
x = Parameter(s) or other variables

Interfacing ATP-EMTP with Matlab is possible, but is time consuming and complicated, but will not be done for this investigation. The other solution would be to solve the DE through integration and then find the roots of the polynomial. Solving the DE through integration was conducted by using an indefinite integral and assuming that the initial conditions were zero. The polynomial obtained is shown by equation 8.

$$G_c = \frac{ln\,|G_c|\,[G_c - i]^2}{\tau_c U_c{}^2} + \frac{4iG_c - G_c{}^2\left[3 + U_c{}^2\right]}{2\tau_c U_c{}^2} \qquad (8)$$

The solution to this equation is also not trivial due to the variable G_c featuring in the natural logarithm and as a square function. The equation does converge for specific values of τ, i and U_c but in order to find the roots either fixed point iteration or Newton methods would be necessary. An application, known as Engineering Equation Solver (EES - [29]), was used to find a solution with various values of the three parameters. It was found that the natural logarithm causes convergence problems. The convergence problems coupled with the assumptions of the initial conditions being zero to find the solution to the polynomial make the solution of the polynomial inaccurate. Therefore it would be necessary to use an application which can solve the D.E., as stated above - Matlab.

Thus due to problems of convergence, difficulties in finding a solution to the Cassie D.E., as well as four unknown parameters a different modelling approach was adopted. It is interesting to note that the original Cassie and Mayr equations give more of a qualitative description of the arc. For the equations to become more meaningful modifications are required, such as introducing more parameters or defining the original parameters in a more general form [24]. These types of modifications make the equations more complicated, and are viable when comparing the mathematical model to laboratory results.

2) Model 2: The second model to be considered is based on the energy balance in the arc column, i.e. it is a form of the Mayr differential equation [30] & [31]. The energy balance equation is shown by equation 9.

$$\frac{dg\,(t)}{dt} = \frac{1}{\tau}\left(G\,(t) - g\,(t)\right) \qquad (9)$$

Where:

g = Instantaneous arc conductance
G = Stationary arc conductance
τ = Arc time constant

This equation may be implemented in ATP-EMTP by using the Laplace transform or as a time domain differential equation.

Two different descriptions of the stationary arc conductance $(G\,(t))$ were found. The first is shown in equation 10 and the second in equation 11

$$G = \frac{|i_{arc}|}{u_{st}l_{arc}} \qquad (10)$$

Where:

$u_{st} = u_o + r_o|i_{arc}|$
u_o = Characteristic arc voltage
r_o = Characteristic arc resistance
i_{arc} = Instantaneous arc current
u_{st} = Stationary arc voltage

$$G = \frac{i_{arc}{}^2}{P_0 + U_0\,|i_{arc}|} \qquad (11)$$

Where:

P_0 = Steady-state heat dissipation
U_0 = Constant percentage of steady-state U-I characteristic
i_{arc} = Instantaneous arc current

To find the characteristic arc resistance and voltage the estimation equations (12 & 13) from [30] were implemented. Other methods to find these two parameters exist, and are generally through the solution of an integral of the instantaneous arc current and conductance [31] & [32]. The simplified equations were developed by Kizilcay [33] and are sufficient for the simulation purposes.

$$U_o = 0.9l_{arc} + 0.4 \qquad (12)$$

$$r_o = 40l_{arc} + 8 \qquad (13)$$

Where:

U_o = [kV]
r_o = [mΩ]

As the length of the arc is dependent on various factors, such wind, the actual arc length is greater that that of the gap length and is a function of time. The arc time constant is directly related to the length of the arc; thus the arc time constant needs to be adjusted accordingly. The correction in the time constant is show by equation 14.

$$\tau = \tau_o \beta^\alpha \qquad (14)$$

Where:

$\beta = \frac{l_{arc}}{l_o}$

l_{arc} = Real arc length [m]

l_o = Physical separation of electrodes [m]

τ_o = Initial time constant [s]

α = Coeffient varying between -0.1 and -0.6

Since there are 3 variables and two equations, another equation is required for the convergence of a solution. The instantaneous current may be calculated by making use of the Thevenin equivalent circuit [30], shown by equation 15.

$$i_{arc} = \frac{g\left(t\right) v_{th}}{1 + g\left(t\right) r_{th}} \tag{15}$$

Therefore the arc conductance, hence the arc resistance, may be found through the simultaneous solution of equations 9, 10 and 15. The second method of solving for the arc conductance is to measure the instantaneous arc current, thus eliminating a variable. The downfall of this method is that the arc conductance is no longer causal (depends on a previous time value of current). The magnitude of inaccuracies of this method will be investigated. The modelling process is discussed further in section III-C.

C. Simulation of the Dynamic Arc Model

Three slightly different variants of Model 2, described in section III-B, were compared. The simulation model used consisted of a 13.6 km distribution line model with 2 parallel branches, each 15 km in length. No surge arrestors were included. The arc model was only implemented on the pole directly struck; none of the other poles were modelled.

In the first two implementations the arc was modelled as a TACS controlled resistance. The current flowing into the TACS resistance was measured thus the stationary arc conductance could be calculated using either equation 10 or 11. The arc conductance was found by solving Equation 9. The arc-over of the insulators and gap is initially dependent on the line voltage exceeding the BIL of the pole, but as the arc forms there is a collapse in voltage. Secondly an unacceptable amount of oscillation in the voltage waveform was found when using a voltage controlled switch. To solve these problems three TACS controlled switches were controlled by a MODELS program, which formed part of the arc modelling program. The line-to-ground voltage was measured before each switch to determine the initial closing conditions. The finer control of the switches made it possible to determine exactly when they should be opened to emulate the extinction of the arc, as well as setting a minimum time that the switches remain closed.

The third implementation used a TYPE-94 MODELS component. This component allows for the supporting circuit to be modeled as a Thevenin or Norton equivalent. The current through the arc can be found by solving equations 9, 10 and 15 simultaneously, by using the TYPE-94 as a Thevenin equivalent and a "'combine iterate'" command. This implementation was found to be computationally expensive and did not produce results deemed as accurate as those from the other two implementations.

The remainder of this section presents results from the first two implementations. In each of the cases presented the arc 'burning' was found to be approximately 700 μs.

1) Implementation 1 - Laplace: The first implementation uses equations 9 and 11, and will be referred to as the power dissipation implementation. Two variants of the implementation of equation 9 were used, namely the Laplace transform and the original D.E. Measurements of interest are the voltage waveforms at the line termination, beginning, and at termination of a parallel branch of the line. The lightning current division between the arc model and the line (both left and right of the arc model) is also examined. Measurements regarding arc voltage and current are also presented. At the point of strike the lightning current splits in three parts; to the right (Figure 22) and left (Figure 23) of strike point along the distribution line, and down the first pole into the arc model (Figure 24). Most of the current follows a path directly down the nearest pole through the arc model, while the proportions travelling either side of the line are significantly less (approximately half either way for the initial 190 μs).
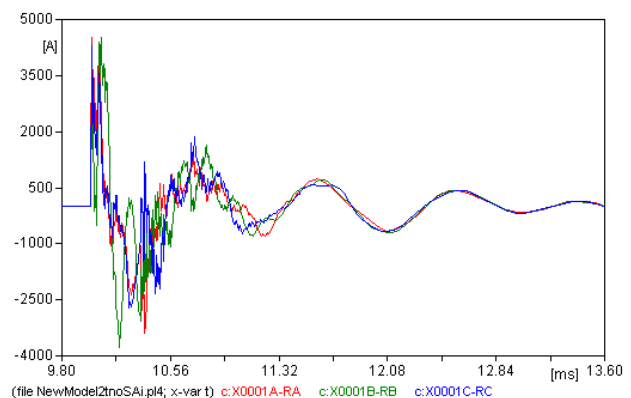
Fig. 22. Current through right hand branch of the distribution line from point of strike - Implementation 1 Laplace

The second set of measurements from this implementation was of the line termination voltage waveforms. Figure 25 shows the voltage waveform measured at the termination point of the second 15 km parallel branch with no arc model included in the simulation. Comparing to Figure 26, which is the measurement at the same point but including the arc model at point of strike, there is a reduction in overvoltage amplitude by approximately 100 kV as well as a very definite change in the waveform. The arc model reduces the ringing, thus adding a degree of stability to the overvoltage waveform.

In terms of the actual arc voltage and current measurements it must be noted that the arc operates in a single phase environment since there is only one wood gap for the three phases. The flashover of each phase was controlled with a TACS switch, as discussed; if the BIL of the phase was
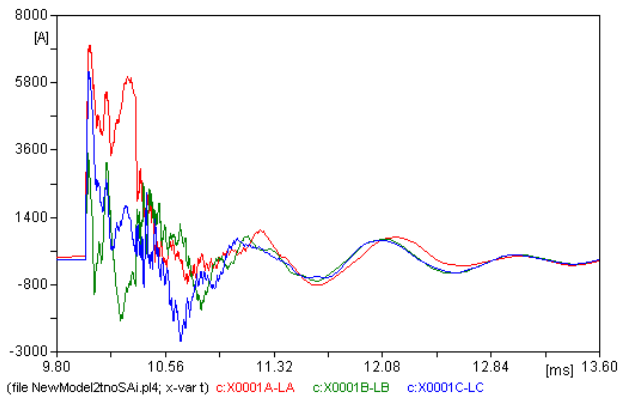
Fig. 23. Current through left hand branch of the distribution line from point of strike - Implementation 1 Laplace
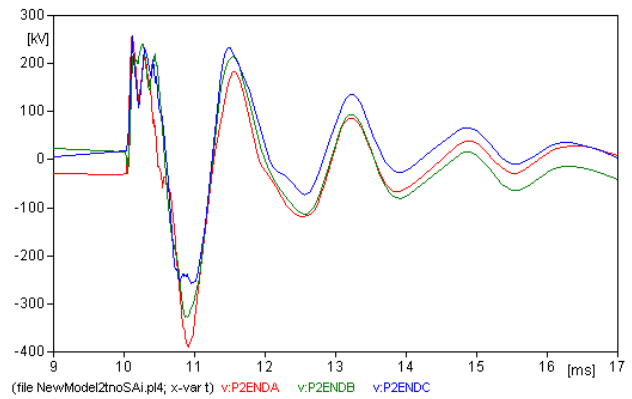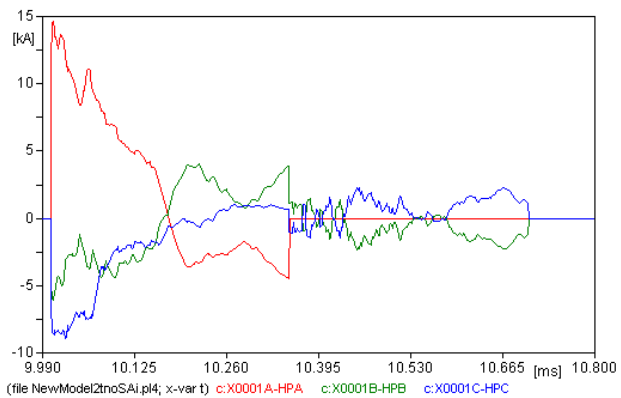
Fig. 24. Current portion to the arc model from point of strike - Implementation 1 Laplace
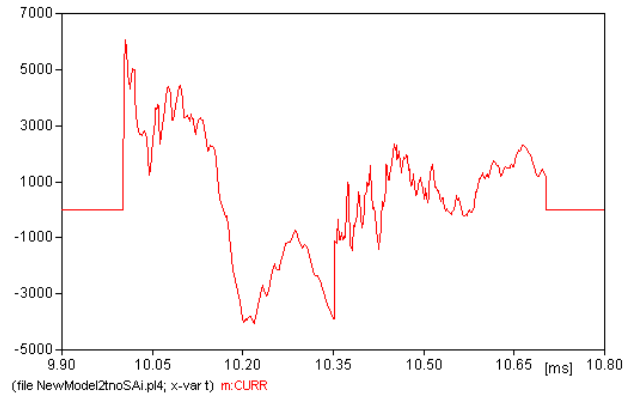
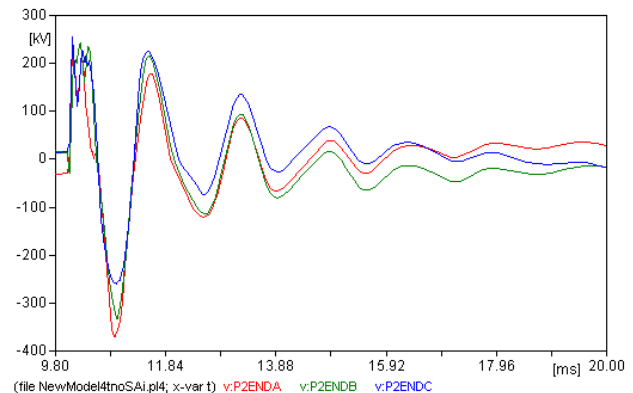Fig. 25. Voltage waveforms measured at the termination of the second parallel branch

Fig. 26. Voltage waveforms measured at the termination of the second parallel branch - Implementation 1 Laplace

Fig. 27. Effective arc current - Implementation 1 Laplace
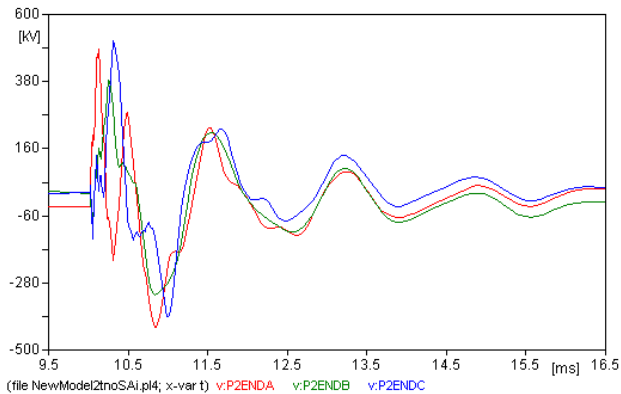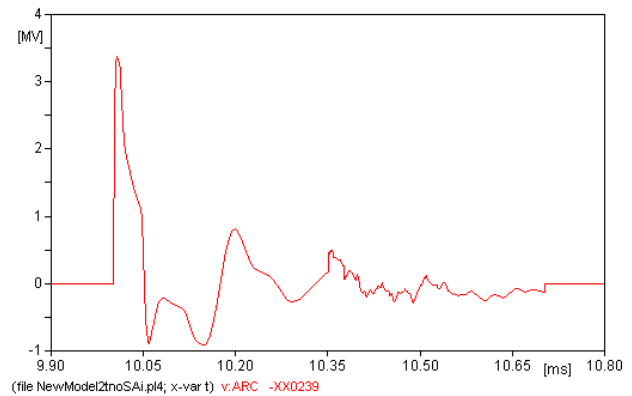
Fig. 28. Effective arc voltage - Implementation 1 Laplace

exceeded then the switch was closed. Thus if all three phases flashed over the resultant current was used as the arc current. This explains why there is a difference between the current measurement in Figure 24 and Figure 27. The effective arc current peaks around 6 kA and steadily decreases with arc duration. It was found that the arc resistance is very high compared to the expected 100 Ohms, thus the arc voltage is very high (Figure 28). The arc resistance was found to be thousands of Ohms.

The variables in equation 11 (P_0 and U_0) were varied and it was found that values for the power dissipation were in the region of 200 kW, and the percentage of steady-state U-I characteristic was 5 kV. These values may not be the optimum for the type of arc being simulated but the only means to finding accurate values would be through laboratory testing.

2) Implementation 1 - D.E.: As a comparison to the results found in from the Laplace solution method shown above,

equation 9 was solved by implementing it as a variable separable D.E. in ATP-EMTP. It would be expected that the results from the two implementations would be almost exactly the same, but there were noticeable differences between the arc current and arc voltage waveforms. Figures 29 and 30 show the current and voltage waveforms, respectively. Comparing to Figures 27 and 28, the current waveforms are similar but the voltage waveforms are completely different, yet the time of arc burning is exactly the same. It is difficult to quantify why the differences are so large in the voltage waveforms. The arc voltage waveform deviates from arc theory and is completely wrong since there is a large negative component when the arc has extinguished. This result shows that this implementation with a differential equation becomes inaccurate. But a comparison of the voltage waveforms measured at the end of the second parallel branch of the line reveals very little difference between the two forms of Implementation 1.
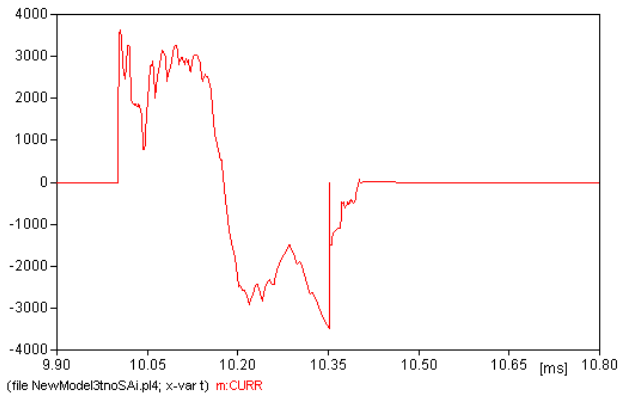
Fig. 29. Effective arc current - Implementation 1 D.E.
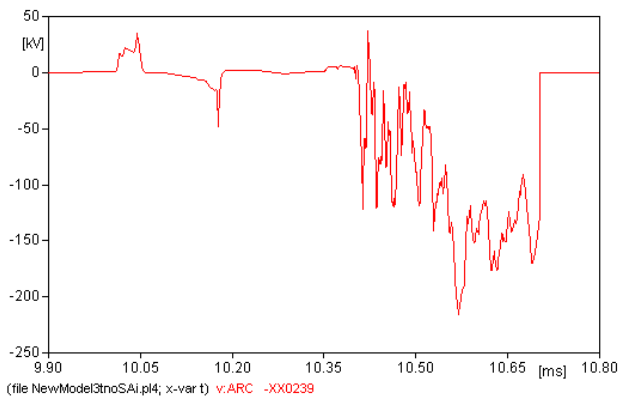
Fig. 30. Effective arc voltage - Implementation 1 D.E.

Figure 31 shows the voltage waveform from the end of the second parallel branch. The amplitude of the first peak is almost 50 kV lower but there is slightly more oscillation. This suggests that the D.E. implementation has a faster response time compared to that of the Laplace implementation. To quantify the vast differences in the arc voltage waveforms it is suspected that further investigation into the power dissipation and initial conditions will yield more conclusive results. Due to the strange arc voltage waveform the accuracy of the D.E.

method cannot be confirmed.

More measurements from the modelling of Implementation 1 - D.E. are available in Appendix II.
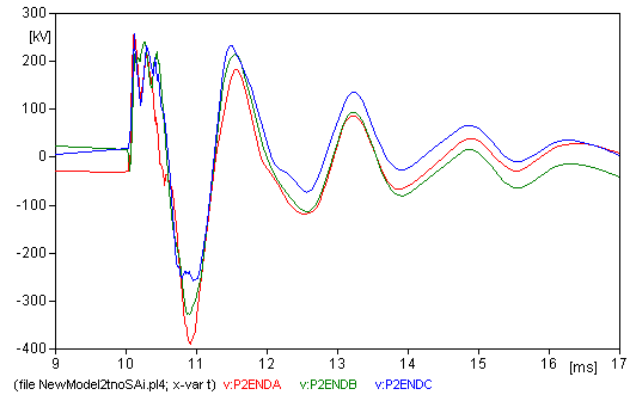
Fig. 31. Voltage waveforms measured at the termination of the second parallel branch - Implementation 1 Laplace

3) Implementation 2 - Laplace: The second implementation makes use of equations 9 and 10. The variables, power dissipation and percentage of steady-state U-I characteristic, are replaced by the stationary arc voltage. The components of this voltage are approximated by Kizilcay [33] from measurements dependent on the arc length. The length of the arc is usually longer than the gap length due environmental factors, but since the arc under investigation is assumed to follow the wood surface between the electrodes, this variation in length is negligible. Thus the length is constant, and the time constant does not change significantly.

The measured waveform at the termination of the second parallel branch (Figure 32) is almost exactly the same as the measurement from the Laplace version of implementation 1, thus indicating that the effects of inaccuracies in the equation variables are minimised over the length of the line.

Fig. 32. Voltage waveforms measured at the termination of the second parallel branch - Implementation 2 Laplace

The arc current (Figure 33) follows a very similar pattern to Figure 27 in terms of waveshape and magnitude for the

initial 10.2 ms. The activity from 10.35 to 10.65 ms is very low and follows a current zero, this is attributed to a miscalculation in the control algorithm which detects the point of arc extinguishment. The arc duration is approximately 600 μs. The arc voltage waveform, shown in Figure 34 was very similar to that shown in Figure 28 in terms of time span and waveshape.

Further measurements from the modelling of Implementation 2 - Laplace are available in Appendix II.

Fig. 35.   Effective arc voltage - Implementation 2 D.E.
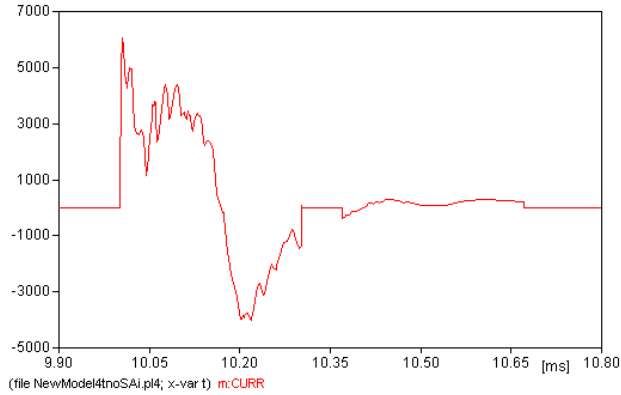
Fig. 33.   Effective arc current - Implementation 2 Laplace

Fig. 36.   Effective arc current - Implementation 2 D.E.
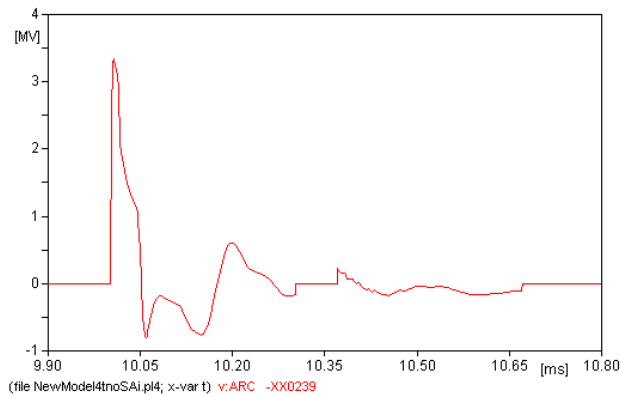
Fig. 34.   Effective arc voltage - Implementation 2 Laplace

4) Implementation 2 - D.E.: The use of the differential equation in this instance provides an arc voltage which is very low compared to the Laplace solution's arc voltage. The arc voltage in this case does not match to the arc current in terms of arc theory. The arc voltage waveform in this implementation is more accurate than that of the D.E. in implementation 1. The arc voltage and current waveforms are shown in Figures 35 and 36, respectively. Due to the inconsistency shown in the voltage waveform the D.E. method will not be used in the full simulation. Other waveform measurements for this implementation are presented in Appendix II.

5) Arc Modelling Summary: The implementations using the Laplace based equations show consistent results. While the implementations using the differential equations provide results which are difficult to quantify in terms of arc theory, thus these two D.E. models will not be used in the full simulation model. Further investigation, through laboratory experimentation, may provide more accurate parameters and inital conditions which could explain the inaccuracies.
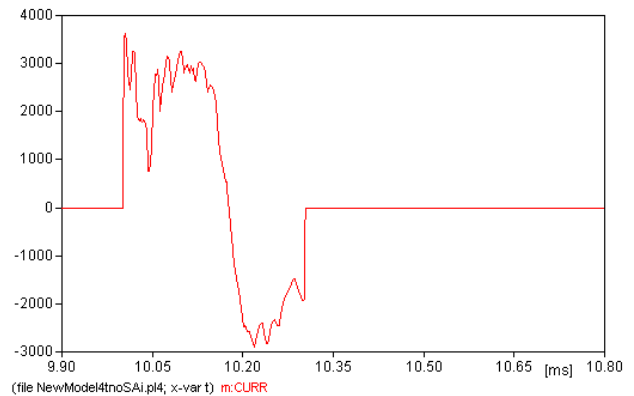
To determine which of the Laplace type implementations to use the simulation results require a slightly more in depth analysis. Implementation 1 will be named Model 1, and Implementation 2 will be named Model 2. Examining the arc voltages; for Model 1 (Figure 28) after 10.35 ms there is significant oscillation when compared to that of Model 2 (Figure 34). The current waveforms mirror the instability in the voltage waveform, from 10.35 ms Figure 27 shows a large 'resonance' in the arc current, the reason for this oscillation is not clear but is a sign of instability. The arc current of Model 2 (Figure 33) shows a very low oscillation in the same time period.

The arc resistance of Model 2 stabilises at 530.38 Ω and the resistance of Model 1 is approximately 3900 Ω, the high resistance of Model 1 does not follow with arc modelling literature which estimate the arc resistance in the region of 100 Ω. Finally, comparing the voltage waveforms at the ends of the parallel branches of the line show that

Model 2 has slightly less oscillation and a marginally lower magnitude to that of Model 1. Therefore Model 2 will be used in the full simulation model presented in the next section.

IV. FULL SIMULATION MODEL

The full simulation model uses equations 9 and 11 to model the arc. Four sets of simulations were conducted, the simulations are divided into two major categories; with and without surge arrestors. Each of these sections is then further subdivided into open circuit and unloaded transformer terminations. For the case of a loaded transformer a per phase load of 3300 Ω to ground was used, this value was used in the transformer modelling process presented in [17]. From all the measurements the differences between loaded and unloaded models was insignificant, therefore only two sets of results are presented and are named as follows:

- Sim 1: No surge arrestors and loaded transformers
- Sim 2: Surge arrestors on the main distribution line with loaded transformers

The arc model is applied to every pole of the struck distribution line; the two parallel branches are modelled only by J. Marti frequency domain line elements and transformer models at their terminations. The models which do not include surge arrestors are used as a control reference, enabling a more accurate analysis of the interaction of different model components. The first aim of the simulation procedure is to show that the arc models provide a noticeable dampening on the overvoltage waveforms, at specific measurement points. The second aim is to confirm the measurements obtained by Eskom (Figure 8) are a direct function of arc quenching action. The Eskom measurements have very little visible surge arrestor action. This suggests that they are from a parallel offset branch of the distribution line rather than the struck line. The simulation results presented focus on the voltage waveforms appearing on the parallel branches, a brief review of the current distribution from the point of strike is also presented. The simulation results discussed below and those obtained from the initial simulation model (section II-H) will be compared in section V.

There are two 15 km branches parallel to the struck distribution line. The first branch has three measurement points, one every 5 km, while the second branch has a measurement point at its termination. Without transformers the overvoltages are expected to reach very high values, this is shown by Figures 37, 38 and 39. As the overvoltage waveform travels the length of the parallel branch the magnitude attenuates with the peak at the termination being 253 kV. Since the over-voltages are high for the initial 15 km of the parallel branch there would be flashover on this segment.

The nature of a distribution line is that it has many branches connected to transformers, and there are surge arrestors installed on each phase of the transformer. Consider Figures 40, 41 and 42 which show the waveforms measured at points on the first parallel branch. In the first 5 km there is significant
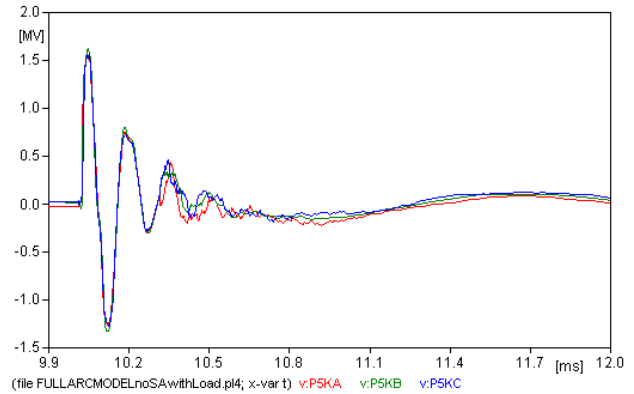
Fig. 37. Voltage waveforms at the 5 km marker on the first parallel branch - Sim 1
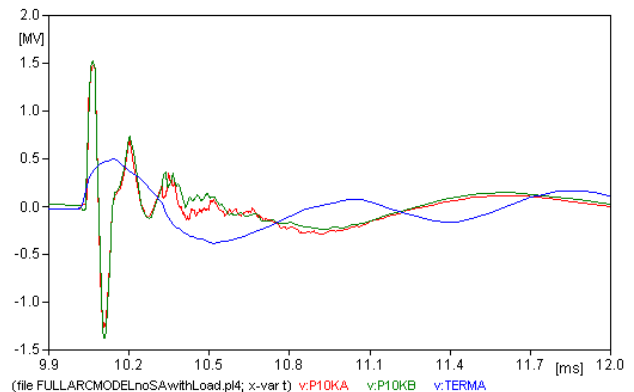
Fig. 38. Voltage waveforms at the 10 km marker on the first parallel branch - Sim 1
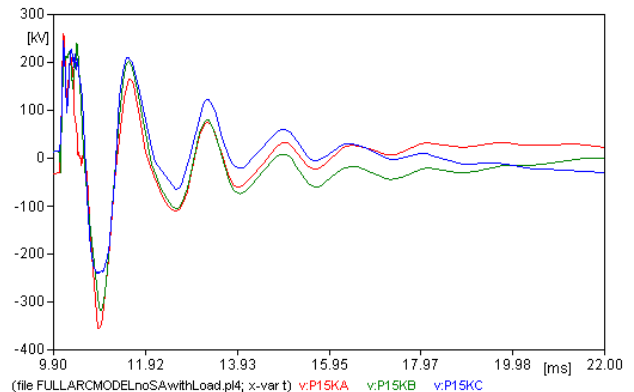
Fig. 39. Voltage waveforms at the 15 km marker on the first parallel branch - Sim 1

oscillation about the first peak, but as the length of the line increases the oscillation is dampened and a single initial peak is visible. The results from the termination of the first parallel branch are identical to those of the termination of the second parallel branch, as expected.

Although the voltages from the second parallel branch are the same as those measured at the termination of the first parallel branch, they are presented in comparison to the no-load conditions. Figure 43 shows the voltage waveform measurement from the termination of the second parallel
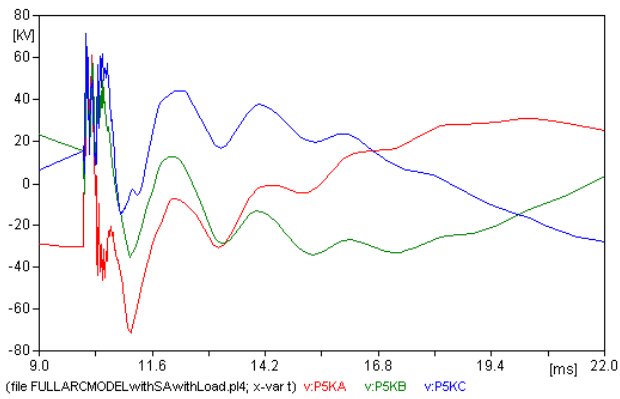
Fig. 40. Voltage waveforms at the 5 km marker on the first parallel branch - Sim 2
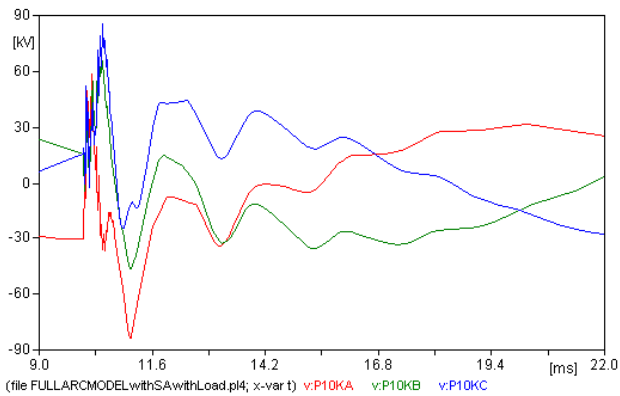
Fig. 41. Voltage waveforms at the 10 km marker on the first parallel branch - Sim 2
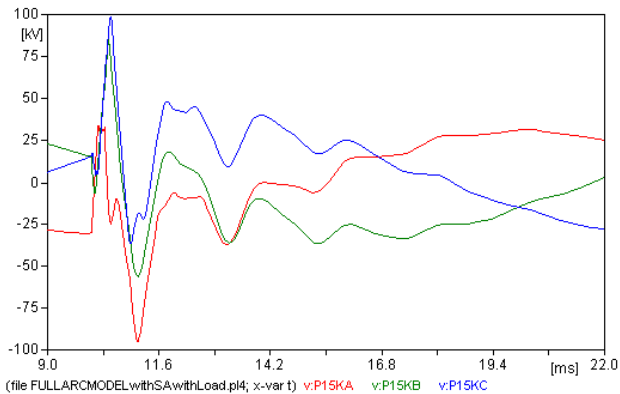
Fig. 42. Voltage waveforms at the 15 km marker on the first parallel branch - Sim 2

branch in Sim 1. The peak magnitude is above 200 kV which is high, but shows that the arc models dampen the lightning overvoltage waveform. For the case of no load the magnitude of the waveforms is expected to drop, and as shown in Figure 45 there is a slight decrease in the magnitude but it is less than 20 kV. The introduction of surge arrestors on the distribution line which is struck should reduce the magnitude of the overvoltage waveform significantly due to arrestor 'action' (dissipation of energy). Figures 44 and 46 confirm that there is a decrease in overvoltage magnitude. As

in the first case there is an insignificant difference between the simulation for the loaded and open circuited simulations. The disturbance time is almost 10 ms before the steady-state voltages and phase sequencing are re-established. Compared to the results from the Eskom measurements the magnitude in the simulations is slightly higher (just above 2 p.u.) but the time response of the measurement is almost identical.
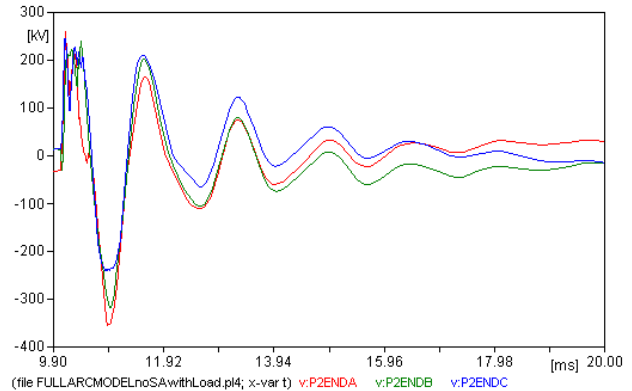
Fig. 43. Voltage waveforms from termination of second parallel branch - Sim 1
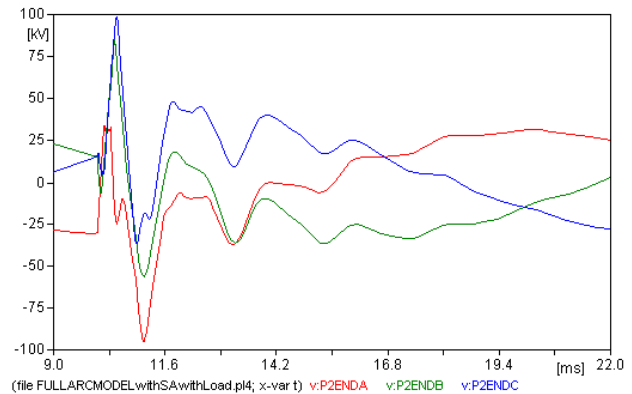
Fig. 44. Voltage waveforms from termination of second parallel branch - Sim 2

Due to the dynamics of all the arc models in the simulation the current distribution from the point of strike changes. For Sim 1, Figures 47 and 48 show the current distribution to the right and left of the point of strike, Figure 49 shows the lightning current component which travels to the first arc model.

There is significant difference between the results from the two simulations. Figure 47 shows two peaks around 10 ms each reaching approximately 5 kA, the waveform has significant oscillation. Only a single current peak would be expected, thus the second peak might be caused by a reflection, but this is not clear from the simulations. Inserting surge arrestors into the model yields Figure 50, at the 10
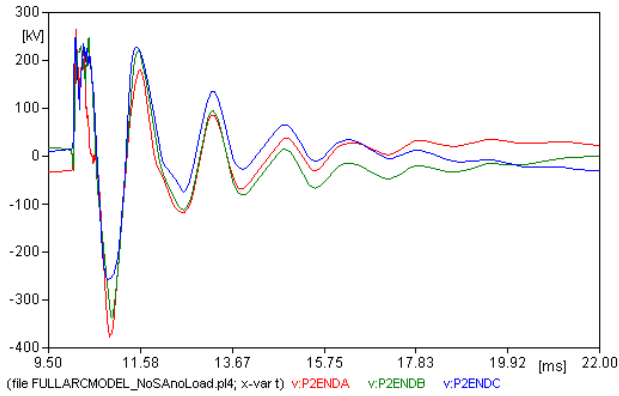
Fig. 45. Voltage waveforms from termination of parallel branch - Sim 1 No load
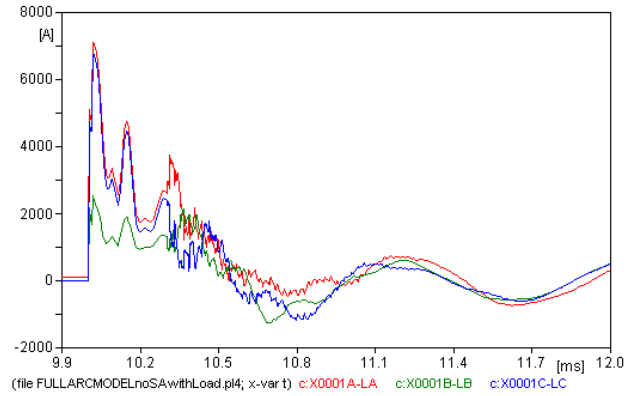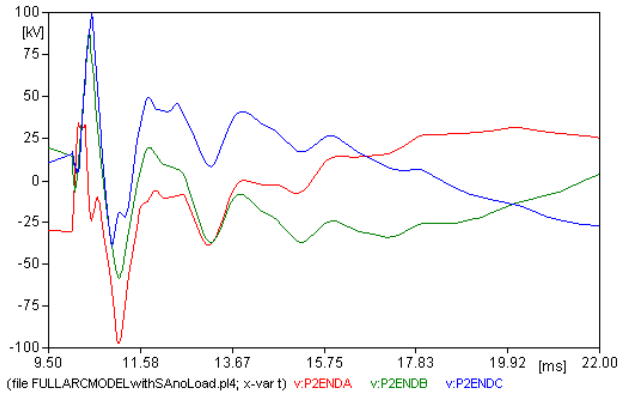
Fig. 46. Voltage waveforms from termination of second parallel branch - Sim 2 no load

Fig. 47. Current waveforms travelling right of the point of strike - Sim 1

Fig. 48. Current waveforms travelling left of the point of strike - Sim 1
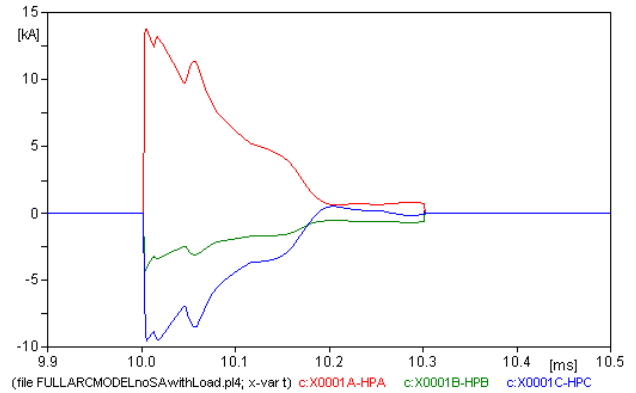
Fig. 49. Current waveforms travelling towards the first arc model - Sim 1
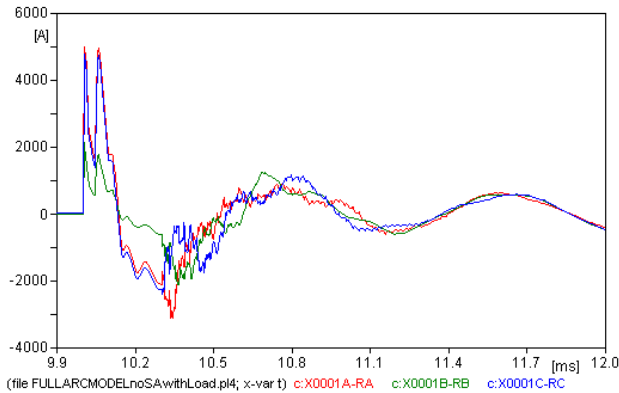
the peak current is higher than that of the case of no surge arrestors, but when closely examined, the resultant current of the three phases is similar for both cases.

Fig. 50. Current waveforms travelling right of the point of strike - Sim 2

ms point there is a single peak, as expected. The oscillation is significantly decreased. The interesting point about this result is that the peak current is higher, but in comparing the two simulation results the average current from 10.0 ms to 10.2 ms is similar. The waveforms travelling to the left of the point of strike show similar behaviour to those that travel to the right. The oscillation in Figure 51 is lower than that of Figure 48 but the current magnitude is higher. Figure 52 shows the current which travels down the closest pole towards the arc model. When surge arrestors are installed
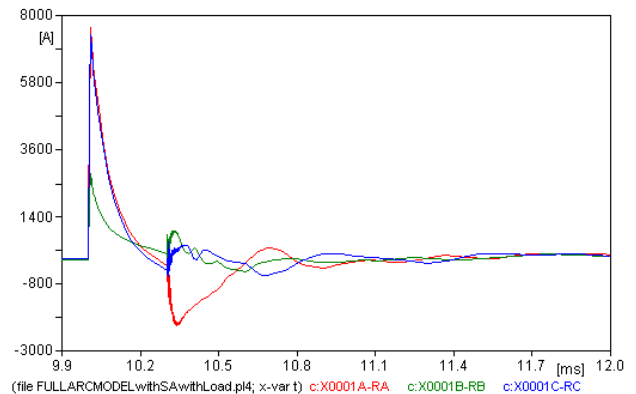
Numerous measurements were conducted for each of the simulation scenarios but are not directly relevant to the purpose of the investigation. These results are presented in Appendix III along with the results for the unloaded transformer cases, and a diagram of the full ATP-EMTP simulation model.
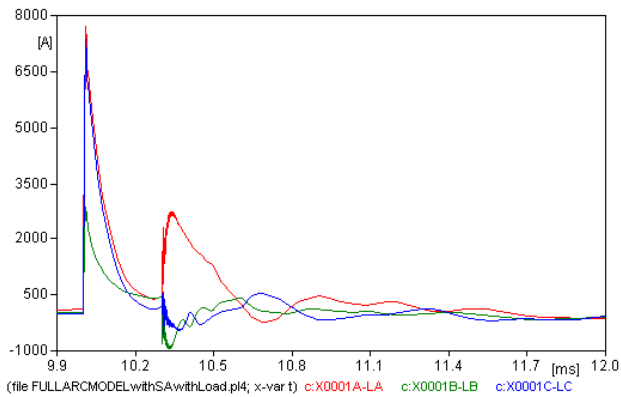
Fig. 51.   Current waveforms travelling left of the point of strike - Sim 2
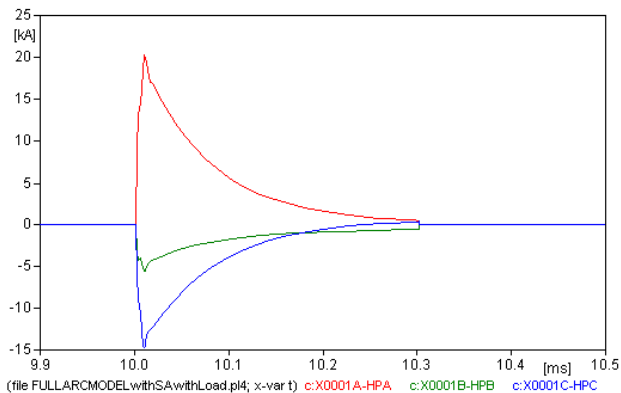
Fig. 52.   Current waveforms travelling towards the first arc model - Sim 2

V. Simulation Results

The comparison of the measured waveforms obtained from the dynamic arc models and static arc models provide valuable insight into the effects of the arc model on the distribution line. The overvoltage waveform at the termination of the parallel branch of the static arc model (Figure 15) has a similar wave shape to that of the dynamic arc model (Figure 44). The dynamic arc model has a slightly lower amplitude (approximately 20 kV). Besides the amplitude, the waveforms are very similar. The other voltage waveforms are also very similar, generally with only small changes in the amplitudes. To quantify the effectiveness of the dynamic arc model the current distribution waveforms need to be examined. The easiest waveform to evaluate is that at the point of strike. Figures 50, 51 and 52 are of the current distribution from the point of strike for the dynamic arc model, Figures 19, 18 and 20 are the current distribution at point of strike for the static arc model.

The current travelling to the right and left along the distribution line away from the point of strike is much higher for the static case by almost double that of the dynamic case. While the current through the arc model is almost three times less for the static model. The static arc model conducts current for approximately 35 μs in comparison to a time of 300 μs for the dynamic model. Thus the dynamic model

dissipates much more energy than the static model.

The final analysis is between the Eskom measurement (Figure 8) and the dynamic arc model measurement at the termination of the parallel branch (Figure 44). The peak amplitude of the Eskom measurement is marginally less than 2 p.u. while the simulation peak amplitude is almost 3 p.u. The difference is accounted to the unknown dynamics of the line and loading. The waveforms are not exactly the same but do follow a similar pattern in terms of peaks and oscillations, the major difference is that most of the peaks are of inverse polarity. The polarity change is attributed to statistical factors surrounding the nature of the lightning stroke. In simulations the most probable worst case lightning stroke was used. The last comparison is the settling time, in the Eskom measurement this time is around 10 ms and in the simulation results it is approximately 9 ms. The simulation results fit closely to the measurement results, this shows that there is definitely not only surge arrestor action but also arc quenching.

VI. Conclusion

The paper has successfully provided a background to the basic configuration of a typical distribution line and the processes which govern the electric arc. Initially a simplistic static arc resistance simulation model was developed and combine into the distribution line model to provide a set of control results which could be used to analyse the more complex dynamic resistance arc model in greater depth. The results were compared to field measurements and it was shown that between the action of arc quenching over a wooden surface (which self-extinguishes) and surge arrestor action the overvoltage waveform may be attenuated sufficiently to prevent switchgear operation. There are many areas in which reasearch on the dynamic arc model can be expanded on, but this will require laboratory experimentation and the use of a simulation program which is capable of dealing with non-variable separable differential equations. In summary, a simplistic dynamic wooden surface arc model was developed which proved sufficiently accurate.

VII. Future Investigations

In the field of electric arc modelling there is much room for future investigation. Generally, any modelling should be accompanied by extensive laboratory experimentation since the dynamics of the arc are very intricate. There are vast quantities of literature which present different types of arc models. Ideally many of the different arc models should be investigated, and then conclusions drawn as to which of the models is the most accurate (or forming a combination of the available models) to create a generalised model.
The capabilities of the simulation package need to be extensive in terms of differential equation solving and iterative solutions.
The final improvement would be to develop a simulation

model which describes a particular test distribution line, rather than making assumptions about the distribution line and then attempting to compare simulation results to measured results. The lightning current source should be modelled to emulate multiple strokes. The effects of indirect lightning strokes may be of interest.

ACKNOWLEDGMENT

REFERENCES

[1] (2006) World-wide mostly used transients program atp-emtp - alternative transients program. Software Application. [Online]. Available: http://www.emtp.org/

[2] J. Swan, P. Crowdy, and J. Maroga, "Eskom distribution standard. part 4: Medium voltage reticulation. section 1: Mv overhead reticulation," Eskom," SCSASAAP1, Feb. 1999.

[3] S.A.B.S., "Protection of structures against lightning. part 1: General principles. section 1: Guide a - selection of protection levels for lightning protection systems," *SABS IEC 1024-1-1:1993*.

[4] "Lightning protection of distribution networks. part ii: Application to mv networks." *CIRFiD/CIGRE Working Group 05 - Protection of MV and LV networks against lightning*, vol. 438.

[5] C. T. Gaunt, A. C. Britten, and H. J. Geldenhuys, "Insulation co-ordination of unshielded distribution lines from 1kv to 36kv," *The High Voltage Co-ordinating Committee. Task Force on the Lightning Protection of Distribution Lines*.

[6] P. P. Barker, T. A. Short, A. R. Eybert-Berard, and J. P. Berlandis, "Induced voltage measurements on an experimental distribution line during nearby rocket triggered lightning flashes," *IEEE Trans. Power Delivery*, vol. 2, pp. 980–995, Apr. 1996.

[7] E. Perez, J. Herrera, and H. Torres, "Sensitivity analysis of induced voltages on distribution lines," *2003 IEEE Bologna Power Tech Conference Proceedings*, vol. 1, p. 7, June 2003.

[8] H. J. Geldenhuys, R. B. Lagesse, A. C. Britten, K. Sadurski, and W. C. van der Merwe, "Practical insulation co-ordination of woodpole distribution lines in high-lightning areas," *3rd AFRICON Conference - AFRICON '92 Proceedings*, pp. 505–508, Sept. 1992.

[9] J. M. Van Coller, "Insulation co-ordination - elen. 584." *School of Electrical and Information Engineering, University of the Witwatersrand*.

[10] "Guide for improving the lightning performance of electric power overhead distribution lines," IEEE, Tech. Rep. 1410-1997, Dec. 1997.

[11] K. Nakada, T. Yokota, S. Yokoyama, A. Asakawa, M. Nakamura, H. Taniguchi, and A. Hashimoto, "Energy absorption of surge arresters on power distribution lines due to direct lightning strokes-effects of an overhead ground wire and installation position of surge arresters," *IEEE Trans. Power Delivery*, vol. 12, pp. 1779–1785, Oct. 1997.

[12] M. F. Stringfellow, "The operating duty of distribution surge arresters due to indirect lightning strikes," *SAIEE Transactions*, vol. 72, pp. 102–122, May 1981.

[13] H. Sugimoto, A. Asakawa, S. Yokoyama, and K. Nakada, "Effectiveness of installing two pairs of distribution surge arresters in parallel," *International Symposium on High Voltage Engineering*, vol. 2, pp. 246–249, Aug. 1999.

[14] IEEE. Working. Group 3.4.11. Application of surge protective devices subcommittee. Surge Protective Devices Committee, "Modeling of metal oxide surge arresters," *IEEE Trans. Power Delivery*, vol. 7, pp. 302–309, Jan. 1992.

[15] P. Pinceti and M. Giannettoni, "A simplified model for zinc oxide surge arresters," *IEEE Trans. Power Delivery*, vol. 14, pp. 393–397, Apr. 1999.

[16] a101435. (2003) The abb group - polim-s..n surge arresters. Internet datasheet. [Online]. Available: http://www.abb.com

[17] A. A. Beutel and J. M. V. Coller, "Surge protection of low voltage power systems for cellular telecommunications sites," *Paper 305 of the IEEE Bologna Powertech*, 2003.

[18] J. D. Cobine, *Gaseous Conductors. Theory and Engineering Applications.* New York: Dover Publications, Inc, 1958.

[19] E. Nasser, *Fundamentals of Gaseous Ionization and Plasma Electronics.* United States of America: John Wiley & Sons, Inc, 1971.

[20] J. M. Somerville, "Introduction to the arc," in *An introduction to discharge and plasma physics*, S. C. Haydon, Ed. Armidale. N.S.W. Australia: Department of University Extension. The University of New England, 1964, ch. 17, pp. 238–244.

[21] H. Maecker, "Theory of thermal plasma and application to observed phenomena," in *An introduction to discharge and plasma physics*, S. C. Haydon, Ed. Armidale. N.S.W. Australia: Department of University Extension. The University of New England, 1964, ch. 18, pp. 245–265.

[22] M. Darveniza, "Electrical breakdown in solids and over solid surfaces," in *An introduction to discharge and plasma physics*, S. C. Haydon, Ed. Armidale. N.S.W. Australia: Department of University Extension. The University of New England, 1964, ch. 9, pp. 152–155.

[23] S. G. Fraser, "Extinguishing the arc," in *An introduction to discharge and plasma physics*, S. C. Haydon, Ed. Armidale. N.S.W. Australia: Department of University Extension. The University of New England, 1964, ch. 23, pp. 344–361.

[24] "Applications of black box modelling to circuit breakers," *Cigre Working Group 13.01 - Electra*, vol. 149, pp. 41–55, Aug. 1993.

[25] L. S. Frost, "Dynamic arc analysis of short-line fault tests for accurate circuit breaker performance specification," *IEEE Trans. on Power App. and Syst.*, vol. PAS-97.

[26] T. E. Browne, "A study of a-c arc behaviour near current zero by means of mathematical models," *AIEE Transactions*, vol. 67.

[27] U. Habedank, "Application of a new arc model for the evaluation of short-circuited breaking tests," *IEEE Trans. Power Delivery*, vol. 8, pp. 1921–1925, Oct. 1993.

[28] (2006) The mathworks - matlab and simulink for technical computing - matlab 7.0.4. Software Application. [Online]. Available: http://www.mathworks.com/

[29] (2006) Ees software - engineering equation solver. Software Application. [Online]. Available: http://www.mhhe.com/engcs/mech/ees/

[30] M. Kizilcay and P. L. Seta, "Digital simulation of fault arcs in medium-voltage distribution networks," *15th PSCC, Liege*, pp. 246–249, Aug. 2005.

[31] L. Prikler, M. Kizilcay, G. Ban, and P. Handl, "Improved secondary arc models based on indentification of arc parameters from staged fault test records," *14th PSCC, Sevilla*, 2002.

[32] Y. Goda, M. Iwata, K. Ikeda, and S. Tanaka, "Arc voltage characteristics of high current fault arcs in long gaps," *IEEE Trans. on Power Delivery*, vol. 15, pp. 791–795, Apr. 2000.

[33] M. Kizilcay and K.-H. Koch, "Numerical fault arc simulation based on power arc tests," *ETEP Journal*, vol. 4, pp. 177–186, May 1994.

Appendix A:

Initial Simulation Results - No Arc Model

This appendix demonstrates the results obtained from the ATP-EMTP distribution line model. Note that this model uses the static arc model.

The first set of measurements is for the system with loaded transformers and no surge protection. The following 5 figures are of the voltage measurements at various points.
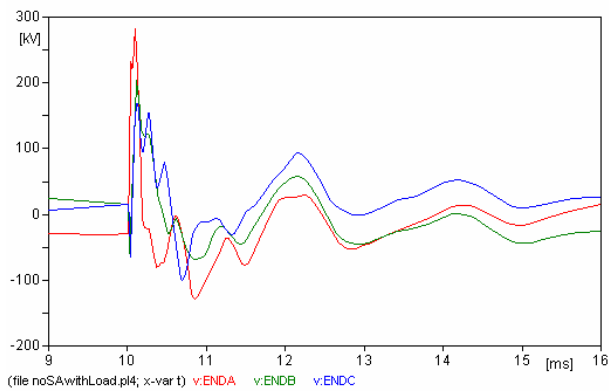
Figure I: Voltage waveform measurement at the end of the distribution line - Static Arc No SA
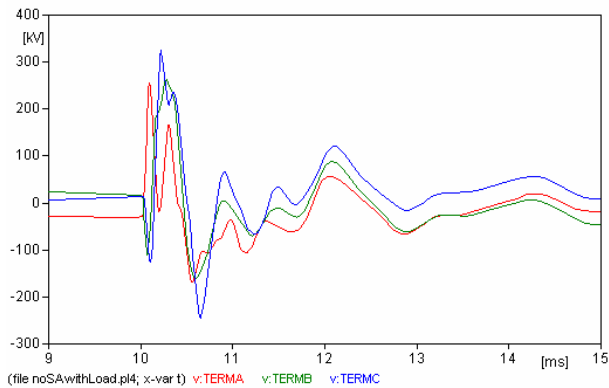
Figure II: Voltage waveform measurement at the termination of the distribution line - Static Arc No SA
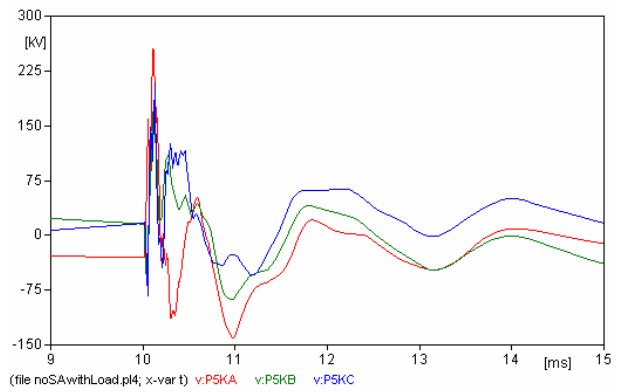
Figure III: Voltage waveform measurement 5 km along the first parallel branch of the distribution line - Static Arc No SA
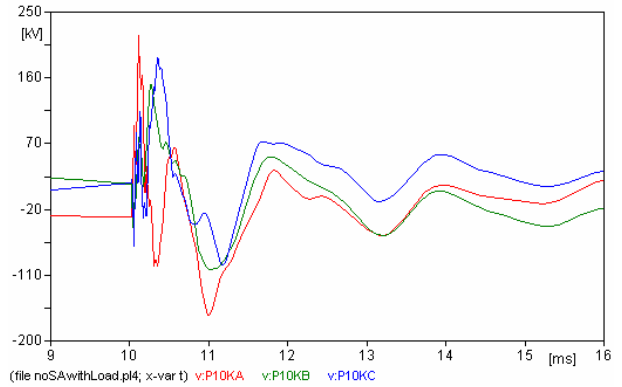
Figure IV: Voltage waveform measurement 10 km along the first parallel branch of the distribution line - Static Arc No SA
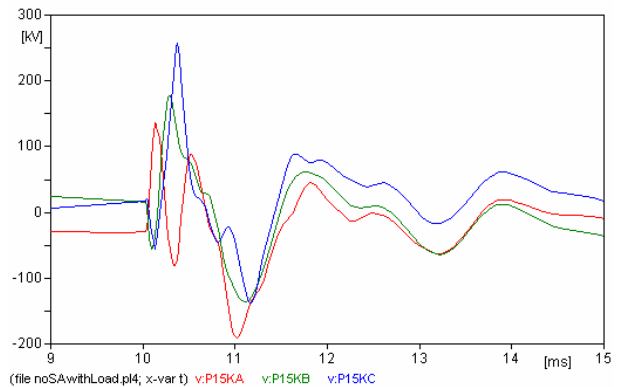
Figure V: Voltage waveform measurement 15 km along the first parallel branch of the distribution line - Static Arc No SA

The next 13 figures are of the current distribution at various points described by the captions.
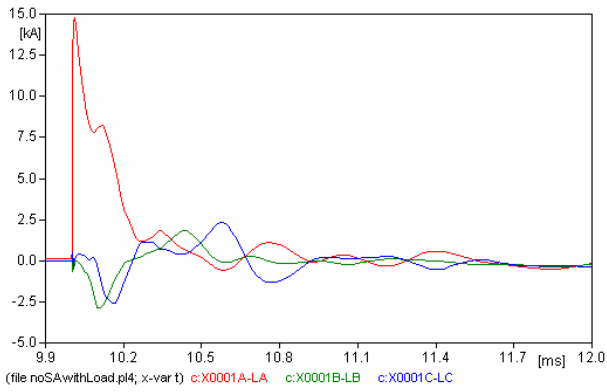
Figure VI: Current waveform travelling left of the point of strike
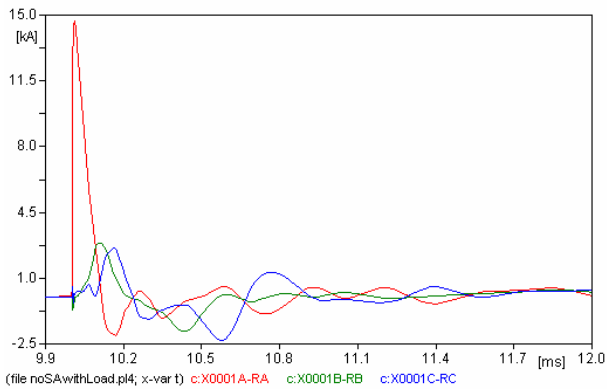
Figure VII: Current waveform travelling right of the point of strike
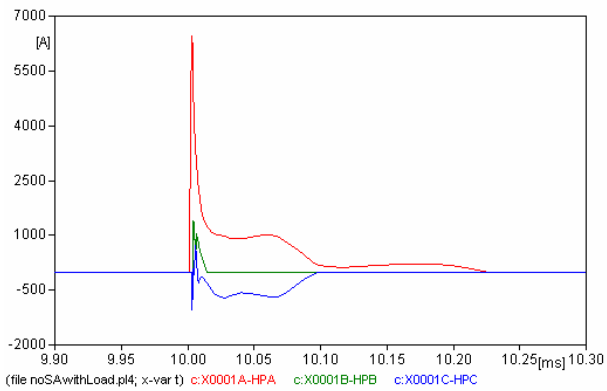
Figure VIII: Current waveform travelling down towards the arc closest to the point of strike
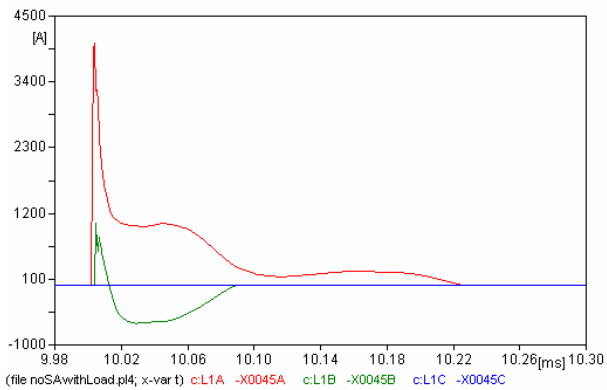
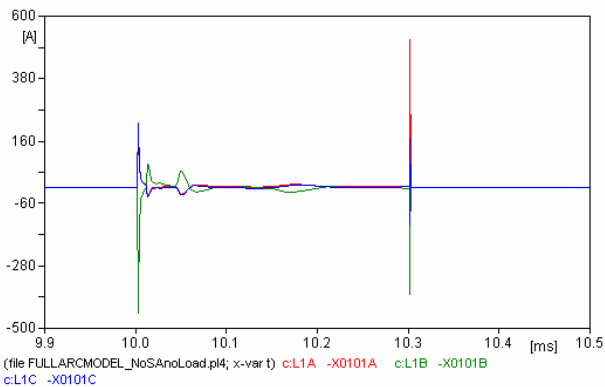**Figure IX: Current waveform travelling down towards the arc of the first pole on the left of the point of strike**
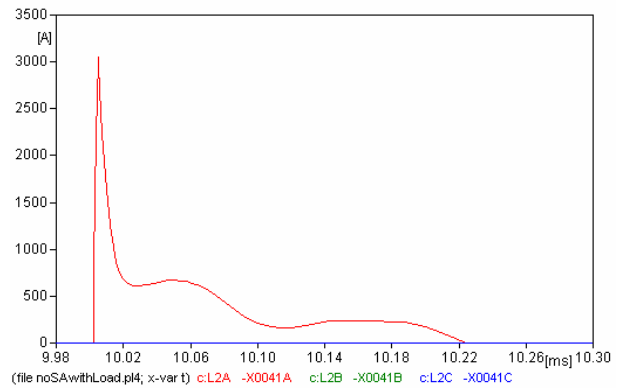
Figure X: Current waveform travelling down towards the arc of the second pole on the left of the point of strike
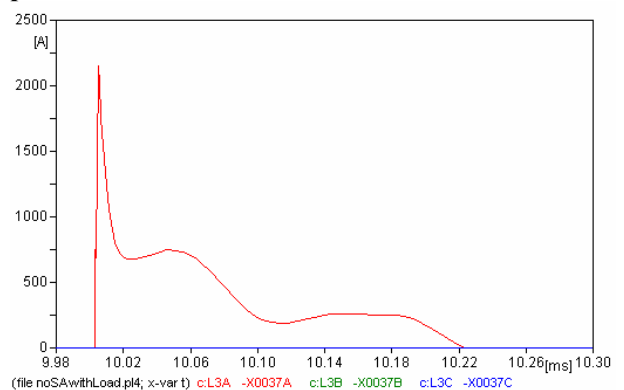
Figure XI: Current waveform travelling down towards the arc of the third pole on the left of the point of strike
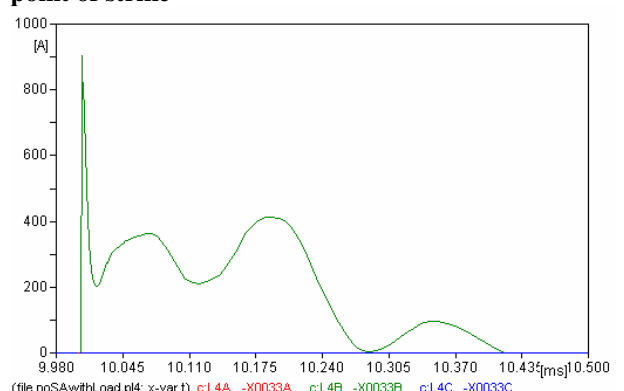
Figure XII: Current waveform travelling down towards the arc of the fourth pole on the left of the point of strike
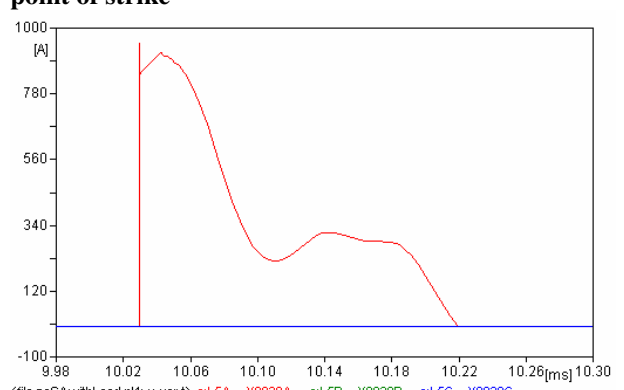
Figure XIII: Current waveform travelling down towards the arc of the fifth pole on the left of the point of strike
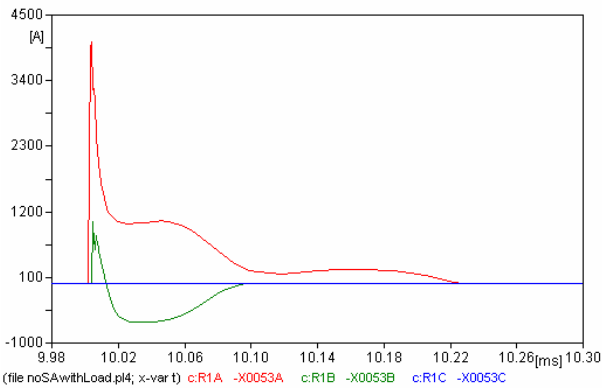
Figure XIV: Current waveform travelling down towards the arc of the first pole on the right of the point of strike
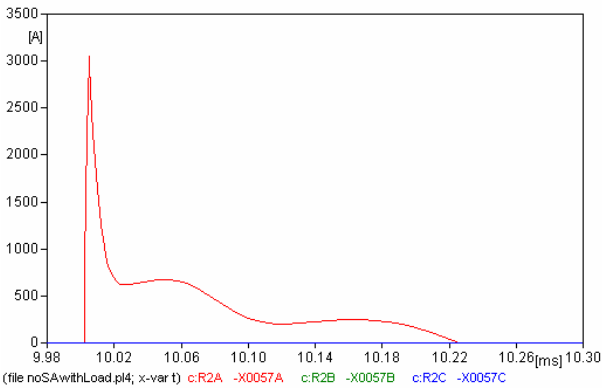
Figure XV: Current waveform travelling down towards the arc of the second pole on the right of the point of strike
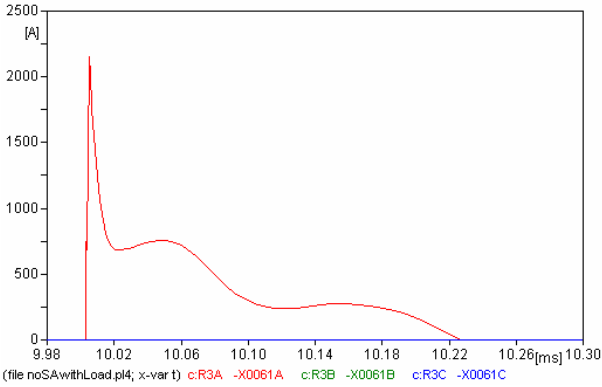
Figure XVI: Current waveform travelling down towards the arc of the third pole on the right of the point of strike
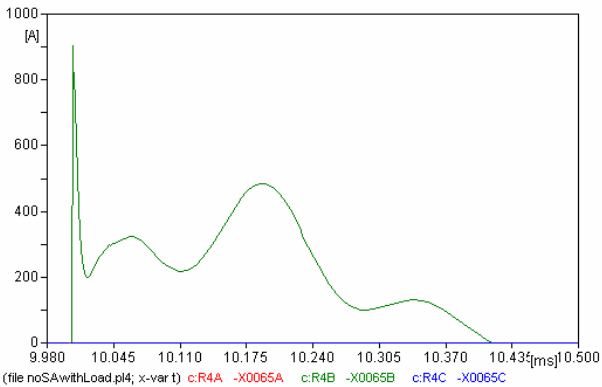
Figure XVII: Current waveform travelling down towards the arc of the fourth pole on the right of the point of strike
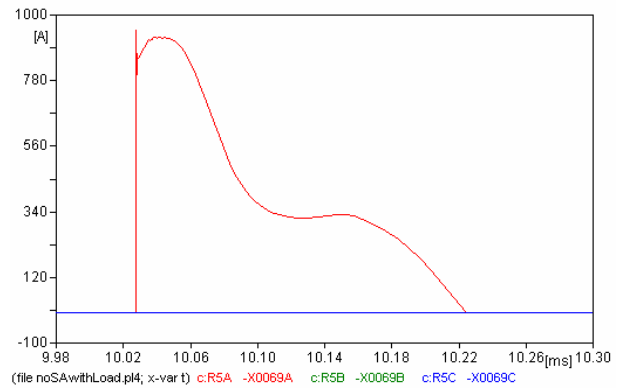
Figure XVIII: Current waveform travelling down towards the arc of the fifth pole on the right of the point of strike

The next set of measurements is from the simulation which has loaded transformers and surge protection installed. Since most of these measurements are included in the main paper only the current distributions to the arcs adjacent to the point of strike are shown.
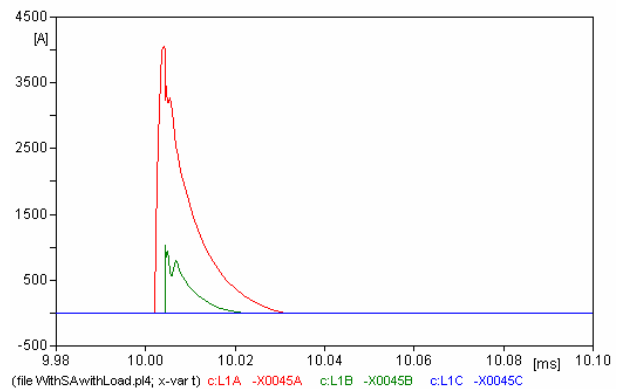
Figure XIX: Current waveform travelling down towards the arc of the first pole on the left of the point of strike
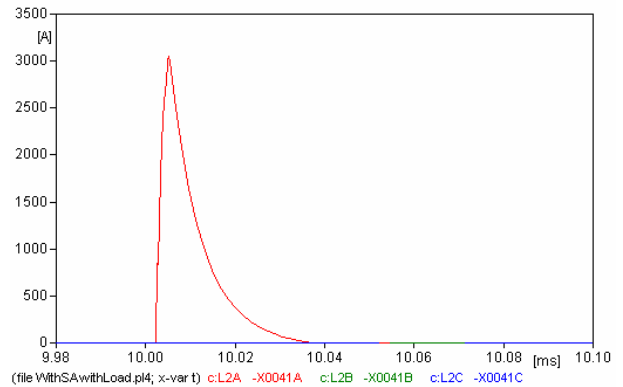
Figure XX: Current waveform travelling down towards the arc of the second pole on the left of the point of strike
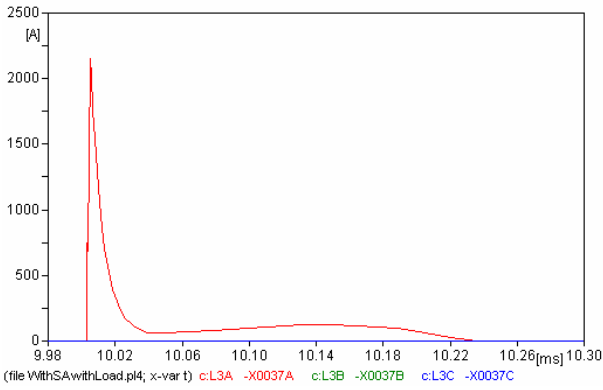
Figure XXI: Current waveform travelling down towards the arc of the third pole on the left of the point of strike
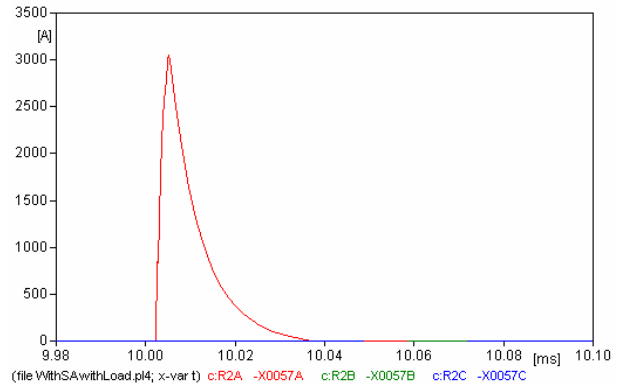
Figure XXV: Current waveform travelling down towards the arc of the second pole on the right of the point of strike
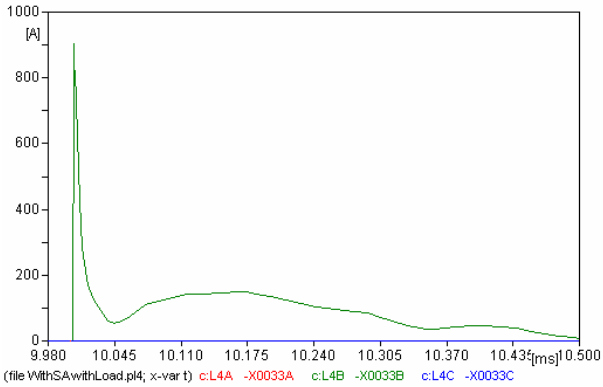
Figure XXII: Current waveform travelling down towards the arc of the fourth pole on the left of the point of strike
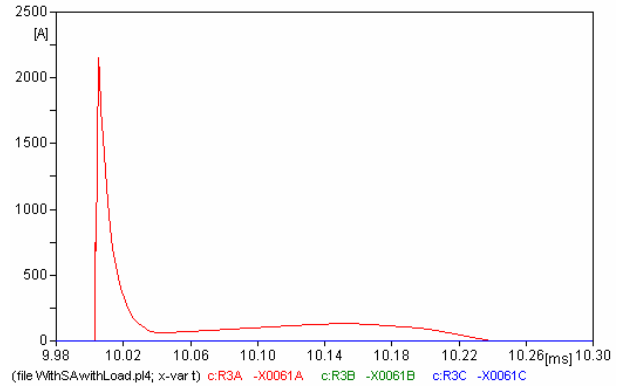
Figure XXVI: Current waveform travelling down towards the arc of the third pole on the right of the point of strike
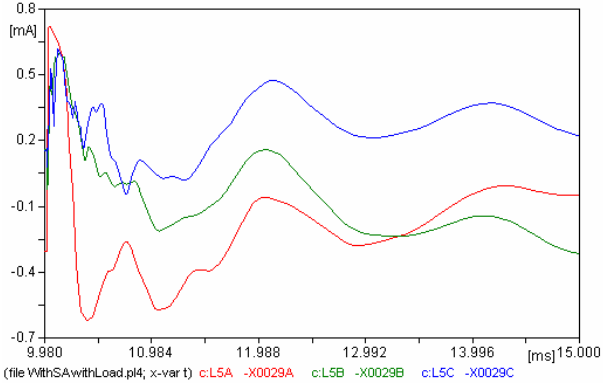
Figure XXIII: Current waveform travelling down towards the arc of the fifth pole on the left of the point of strike
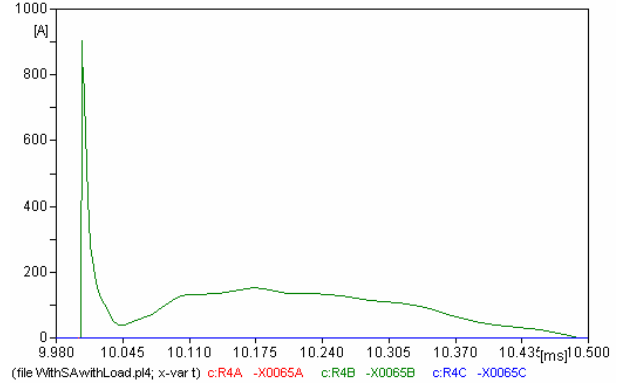
Figure XXVII: Current waveform travelling down towards the arc of the fourth pole on the right of the point of strike
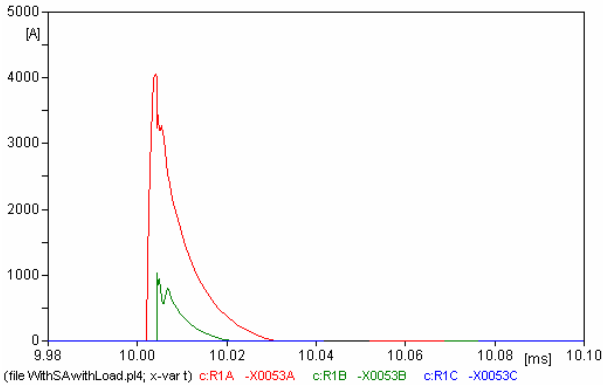
Figure XXIV: Current waveform travelling down towards the arc of the first pole on the right of the point of strike
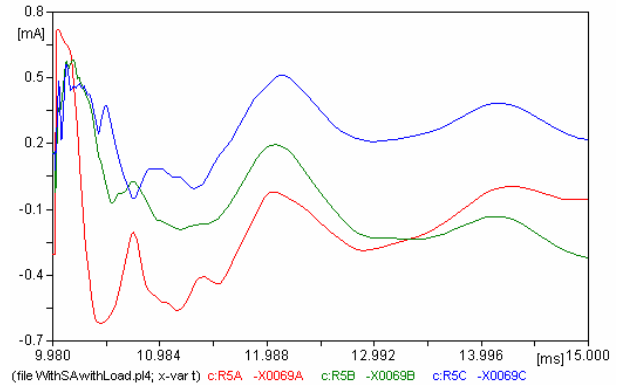
Figure XXVIII: Current waveform travelling down towards the arc of the fifth pole on the right of the point of strike

Appendix B:

Further Measurement Results from the Simulation Arc Model

Measurements from implementation 1 - D.E. are shown in the following six figures. The next six figures are of similar measurements taken in implementation 2 - Laplace. The final seven figures are from Implementation 2 - D.E. Each of the figures has a short caption which describes its origins.
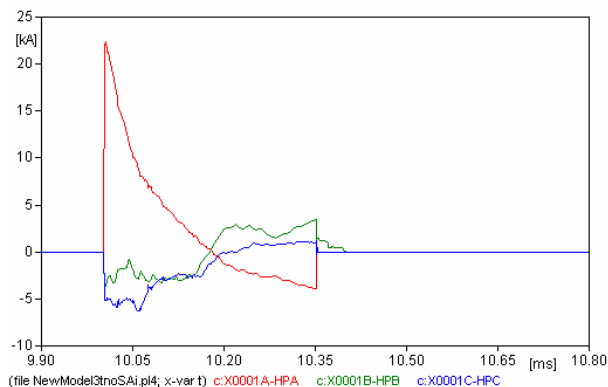
Figure I: Current waveforms travelling towards the arc model from point of strike - Implementation 1 D.E.
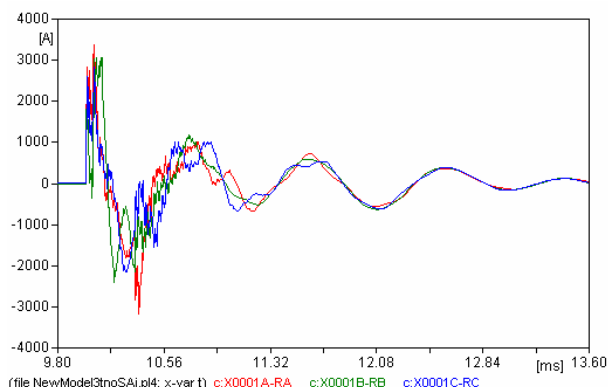
Figure II: Current waveforms travelling to the right of the point of strike - Implementation 1 D.E.
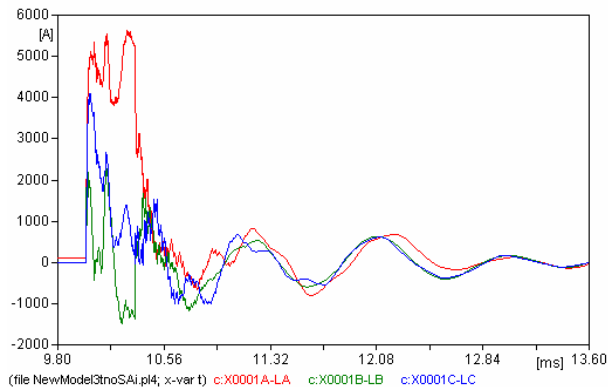
Figure III: Current waveforms travelling to the left of the point of strike - Implementation 1 D.E.
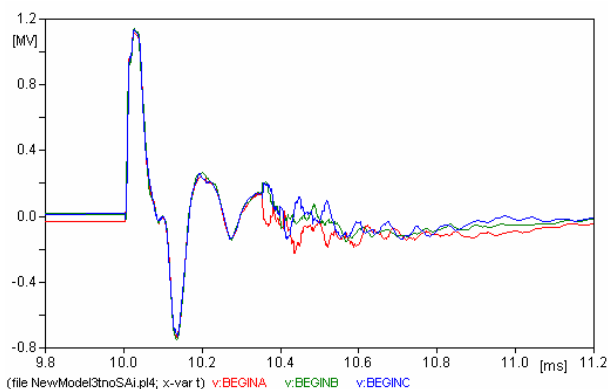
Figure IV: Voltage waveform measurement at the beginning of the distribution line - Implementation 1 D.E.
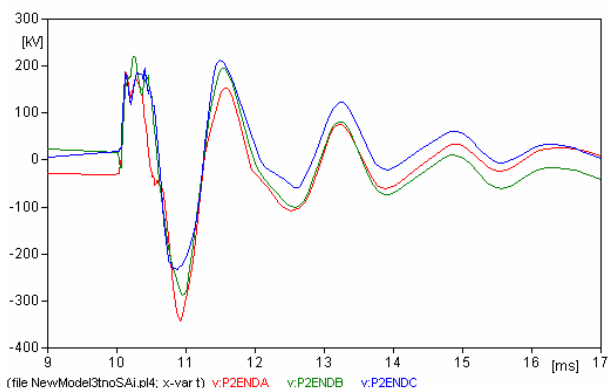

Figure V: Voltage waveform measurement at the end of the distribution line - Implementation 1 D.E.
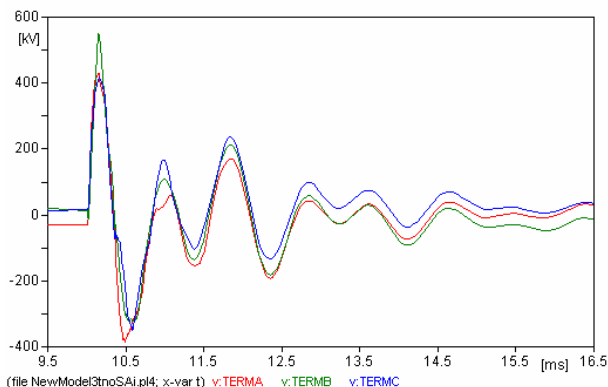
Figure VI: Voltage waveform measurement at the termination point of the distribution line - Implementation 1 D.E.

Implementation 2 – Laplace
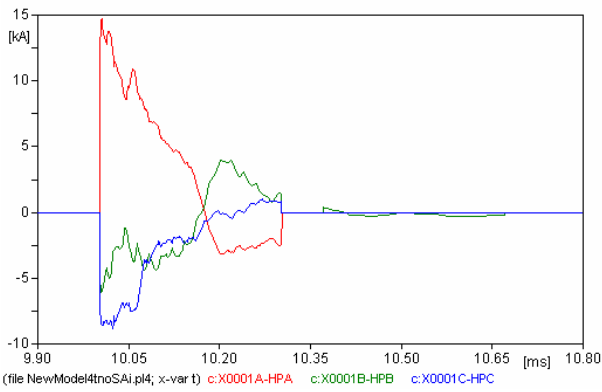
Figure VII: Current waveforms travelling towards the arc model from point of strike - Implementation 2 Laplace
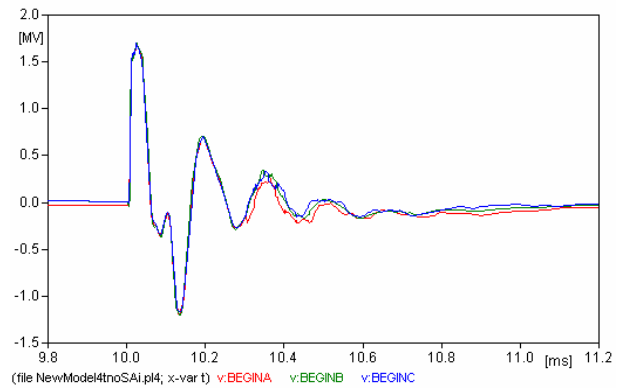
Figure X: Voltage waveform measurement at the beginning of the distribution line - Implementation 2 Laplace
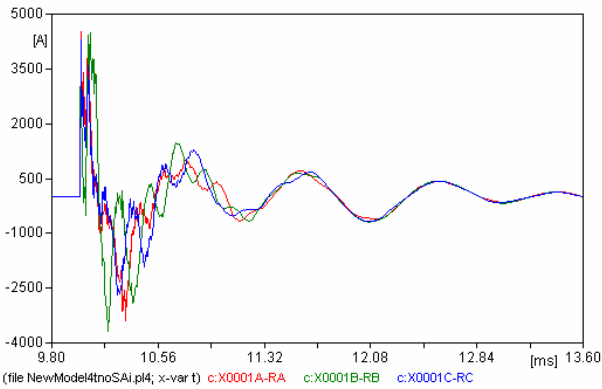
Figure VIII: Current waveforms travelling to the right of the point of strike - Implementation 2 Laplace
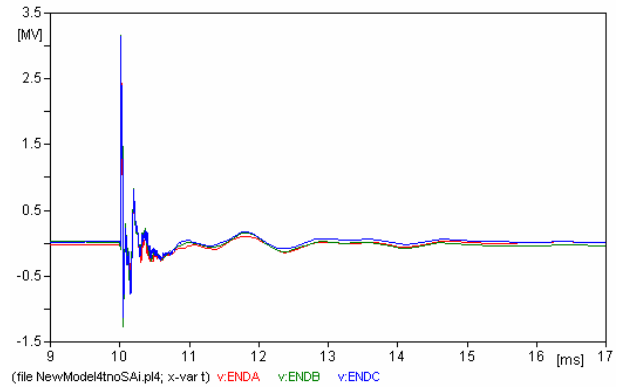
Figure XI: Voltage waveform measurement at the end of the distribution line - Implementation 2 Laplace
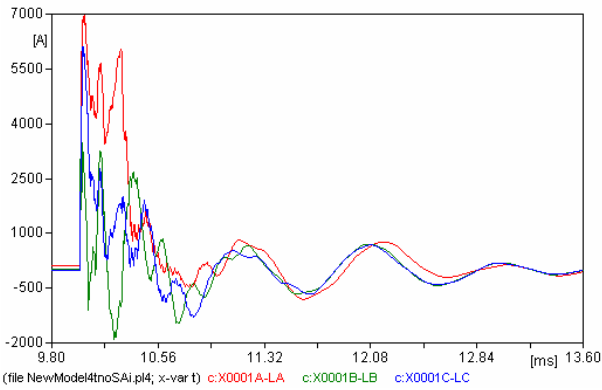
Figure IX: Current waveforms travelling to the left of the point of strike - Implementation 2 Laplace
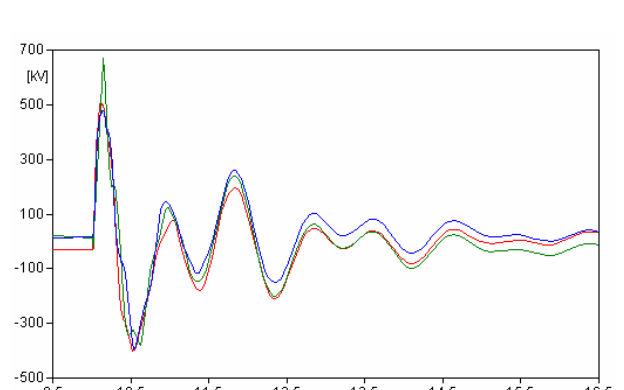
Figure XII: Voltage waveform measurement at the termination point of the distribution line - Implementation 2 Laplace

Implementation 2 – D.E.
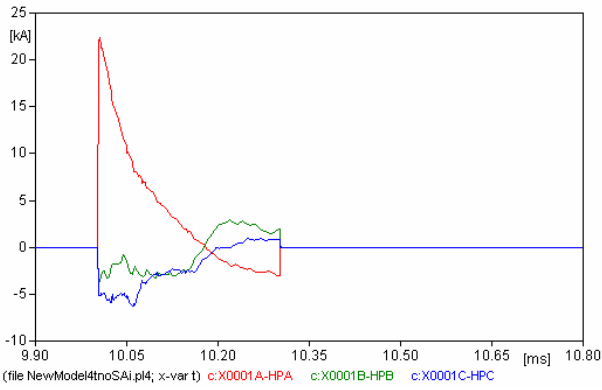
Figure XIII: Current waveforms travelling towards the arc model from point of strike - Implementation 2 D.E.

Figure XIV: Current waveforms travelling to the right of the point of strike - Implementation 2 D.E.

Figure XV: Current waveforms travelling to the left of the point of strike - Implementation 2 D.E.

Figure XVI: Voltage waveform measurement at the beginning of the distribution line - Implementation 2 D.E.
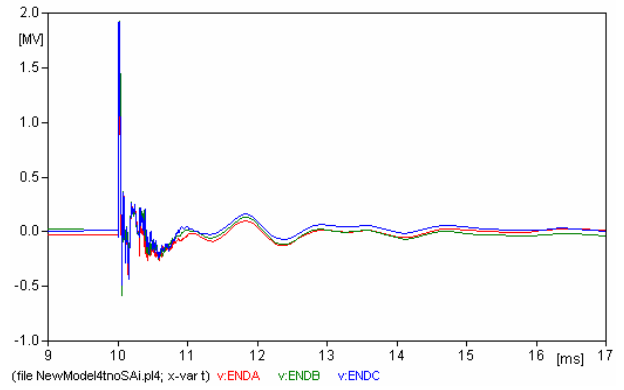
Figure XVII: Voltage waveform measurement at the end of the distribution line - Implementation 2 D.E.
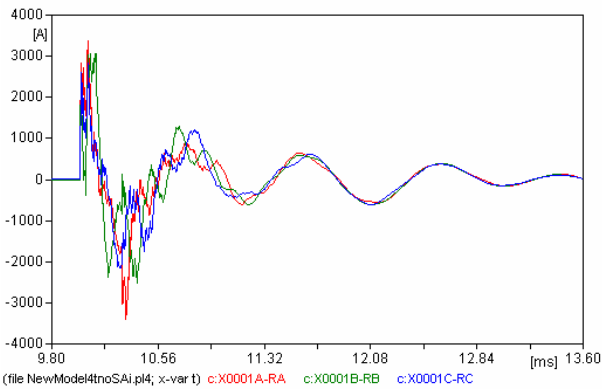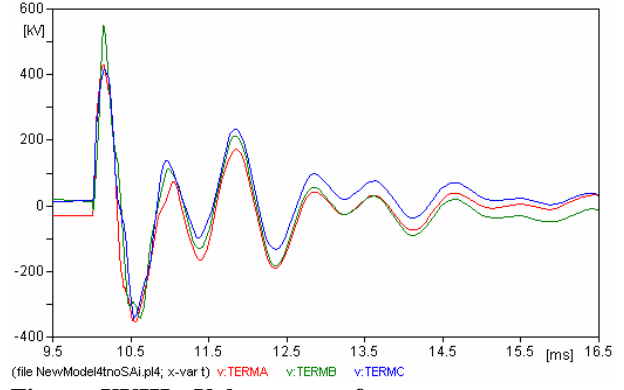
Figure XVIII: Voltage waveform measurement at the termination point of the distribution line - Implementation 2 D.E.

Appendix C:

Further Measurement Results from the Full Simulation

Each of the following four sets of measurements begins with the voltage measurements from the parallel branches, voltage measurements from the struck distribution line, current distribution measurements about the point of strike, and finally a set of current measurements taken before the first six poles on either side of the point of strike. Each set of the measurements only contains figures which were not included in the main paper.

The first set of figures is of Sim 1 but with unloaded transformers.
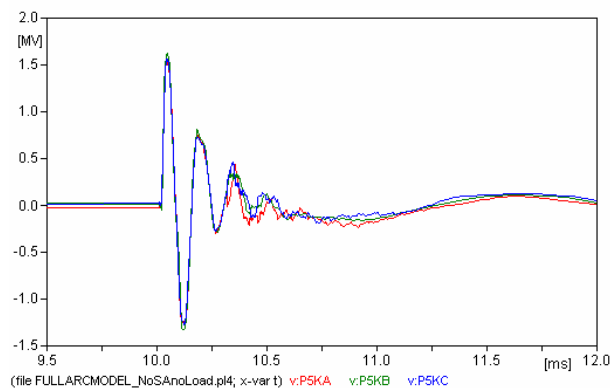
Figure I: Voltage waveform measurement at the 5 km measurement point on parallel branch 1 - Sim 1 No load
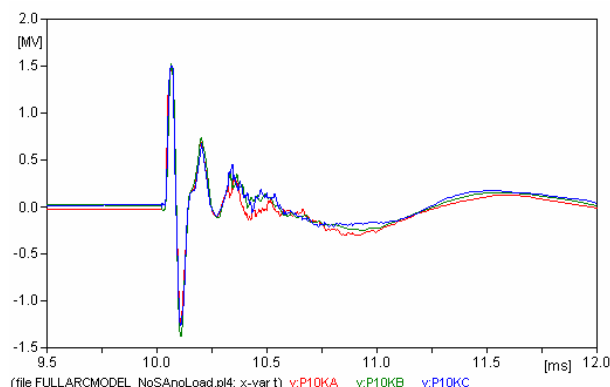
Figure II: Voltage waveform measurement at the 10 km measurement point on parallel branch 1 - Sim 1 No load
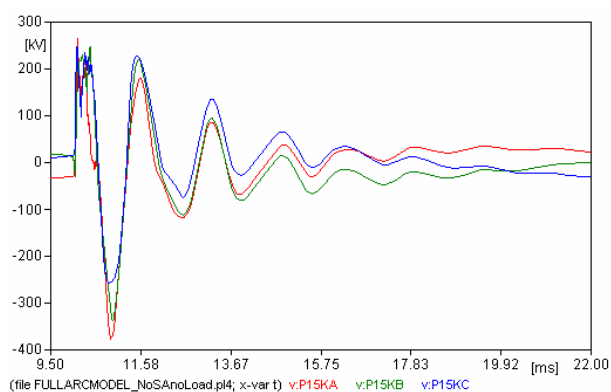
Figure III: Voltage waveform measurement at the 15 km measurement point on parallel branch 1 - Sim 1 No load
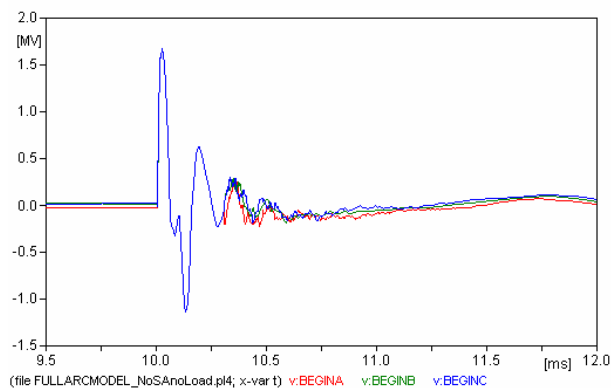
Figure IV: Voltage waveform measurement at the point of split to the parallel lines - Sim 1 No load
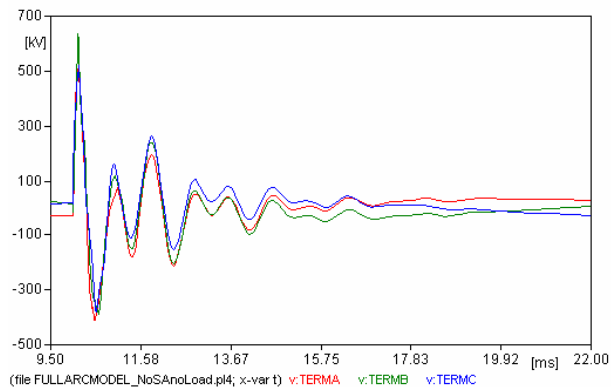
Figure V: Voltage waveform measurement at the termination of the main distribution line - Sim 1 No load
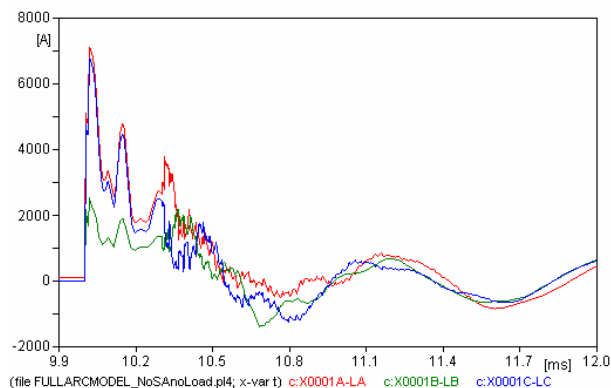
Figure VI: Current waveform travelling left of the point of lightning strike - Sim 1 No load
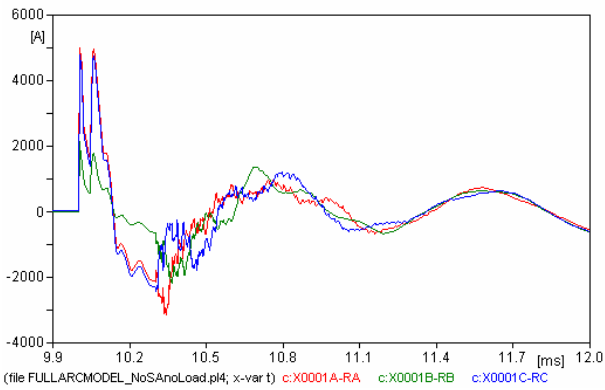
Figure VII: Current waveform travelling right of the point of lightning strike - Sim 1 No load
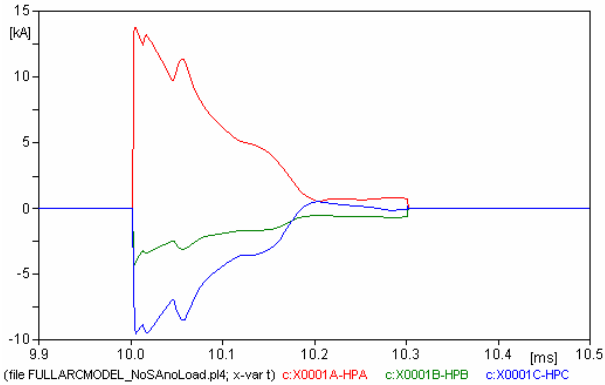
Figure VIII: Current waveform travelling down the pole nearest the point of lightning strike - Sim 1 No load

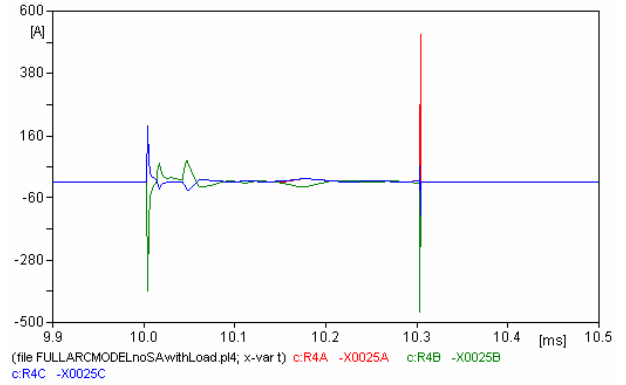**Figure IX: Current waveform travelling to the arc on the first pole on the left of point of lightning strike - Sim 1 No load**
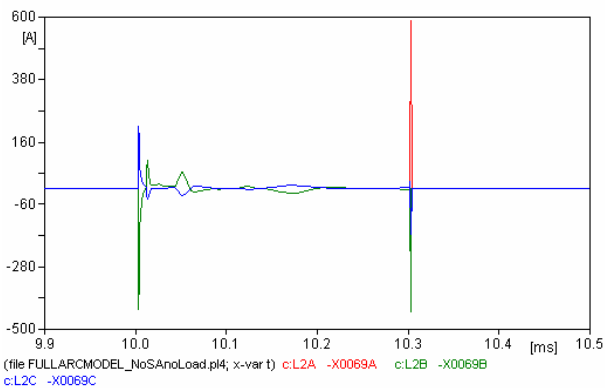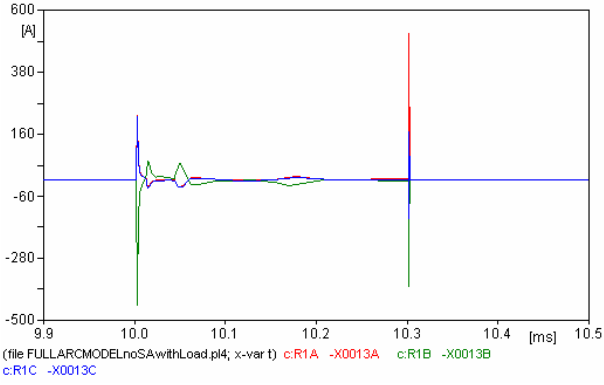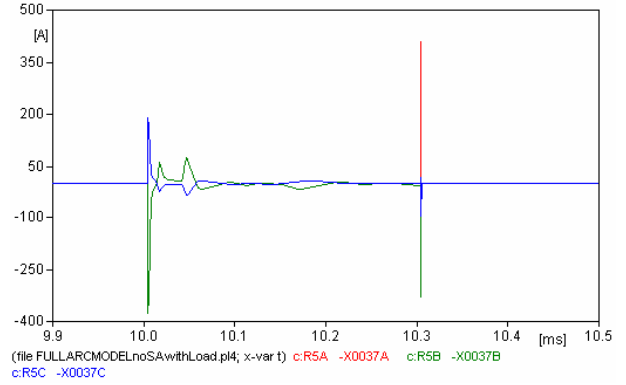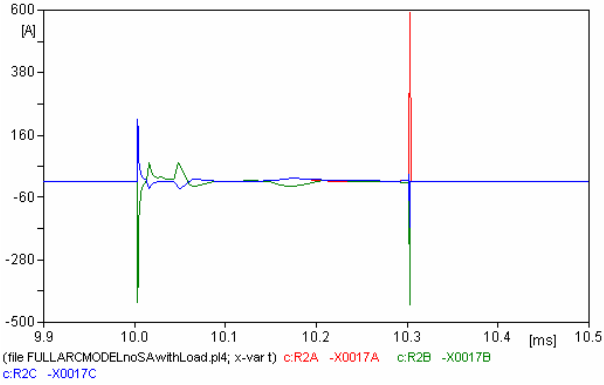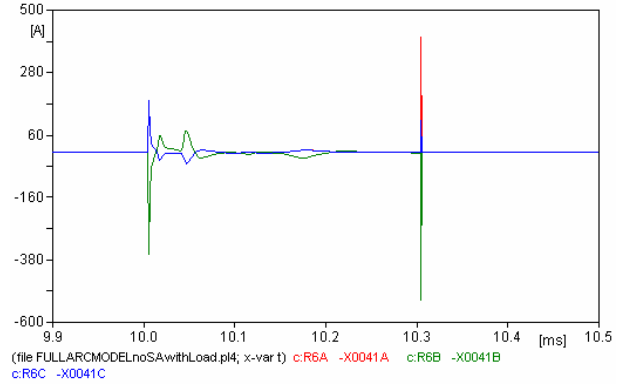

**Figure X: Current waveform travelling to the arc on the second pole on the left of point of lightning strike - Sim 1 No load**
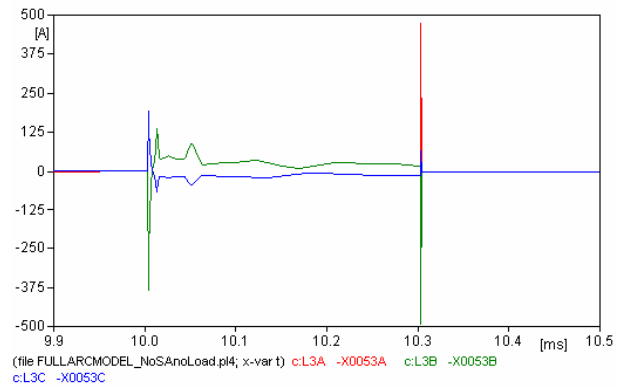

Figure XI: Current waveform travelling to the arc on the third pole on the left of point of lightning strike - Sim 1 No load
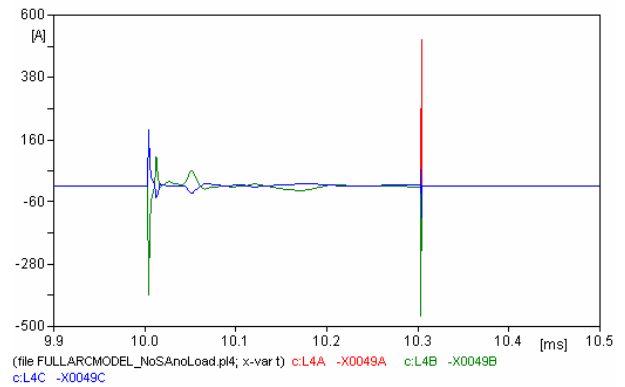

Figure XII: Current waveform travelling to the arc on the fourth pole on the left of point of lightning strike - Sim 1 No load
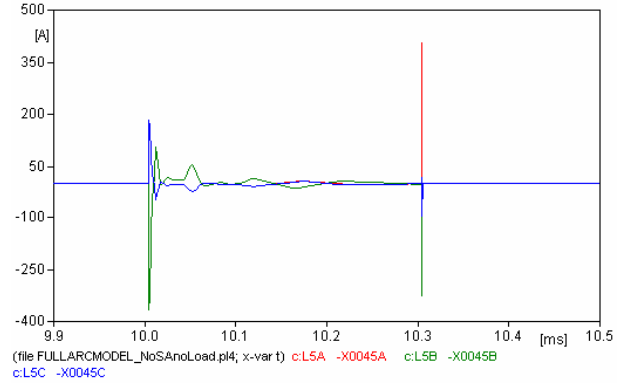
Figure XIII: Current waveform travelling to the arc on the fifth pole on the left of point of lightning strike - Sim 1 No load
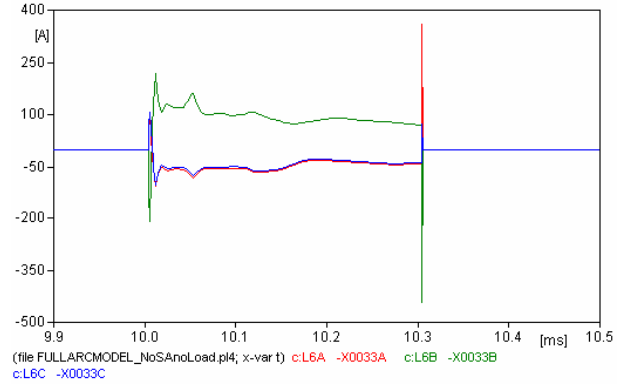
Figure XIV: Current waveform travelling to the arc on the sixth pole on the left of point of lightning strike - Sim 1 No load
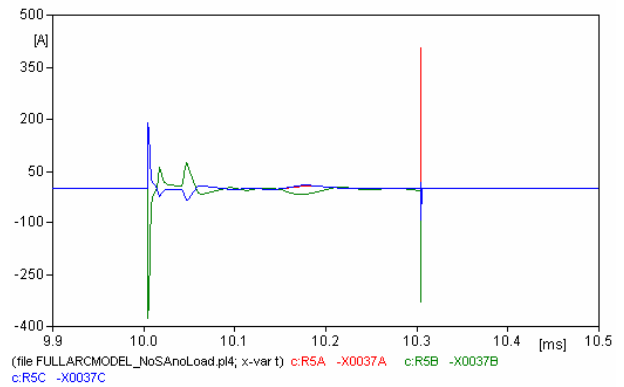
Figure XV: Current waveform travelling to the arc on the first pole on the right of point of lightning strike - Sim 1 No load
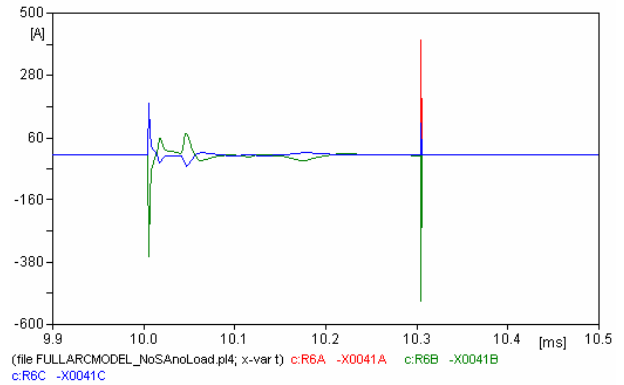
Figure XVI: Current waveform travelling to the arc on the second pole on the right of point of lightning strike - Sim 1 No load

Figure XVII: Current waveform travelling to the arc on the third pole on the right of point of lightning strike - Sim 1 No load

Figure XVIII: Current waveform travelling to the arc on the fourth pole on the right of point of lightning strike - Sim 1 No load

Figure XIX: Current waveform travelling to the arc on the fifth pole on the right of point of lightning strike - Sim 1 No load
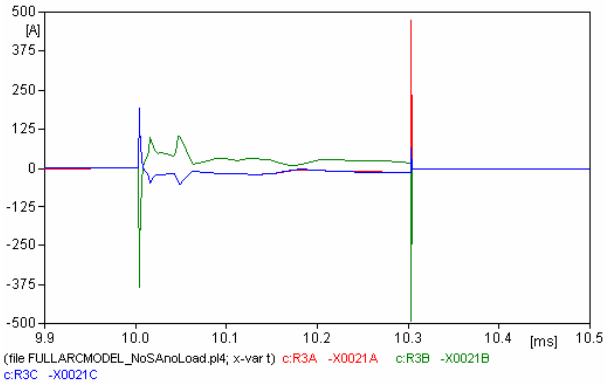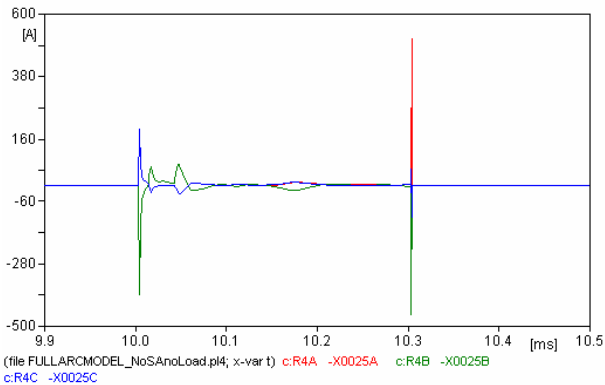
Figure XX: Current waveform travelling to the arc on the sixth pole on the right of point of lightning strike - Sim 1 No load

The second set of figures is of Sim 1.
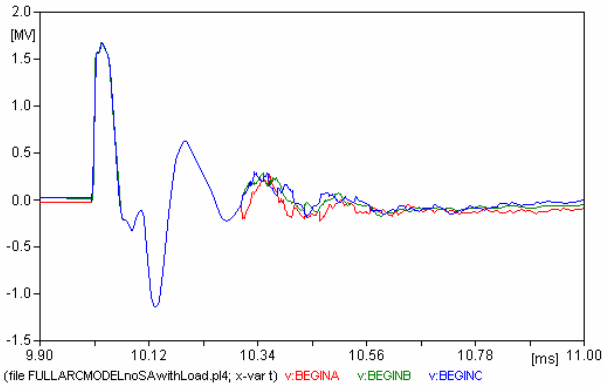
Figure XXI: Voltage waveform measurement at the point of split to the parallel lines - Sim 1 loaded
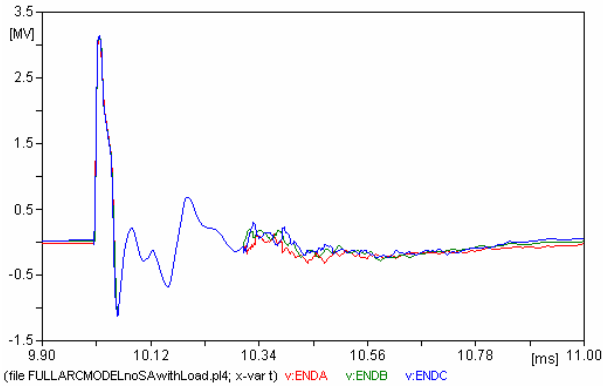
**Figure XXII: Voltage waveform measurement at the end of the struck distribution line - Sim 1 loaded**
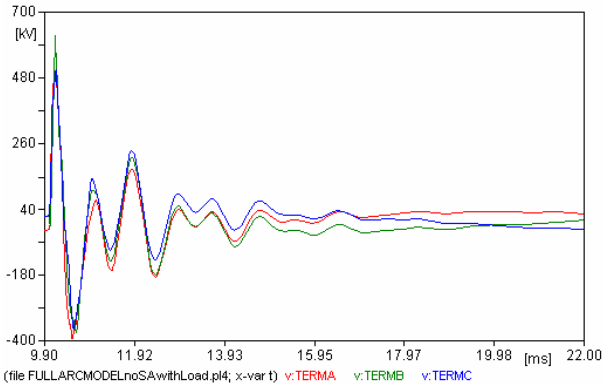

Figure XXIII: Voltage waveform measurement at the termination of the main distribution line - Sim 1 loaded
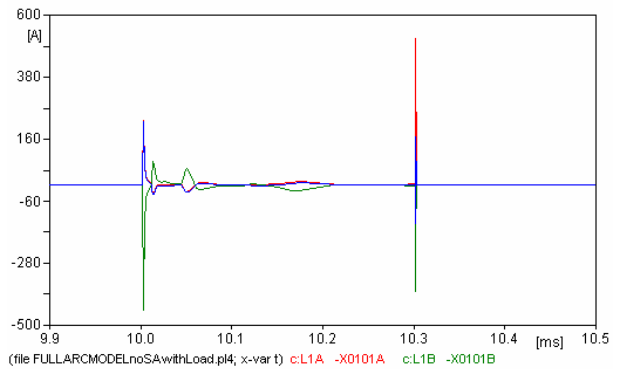
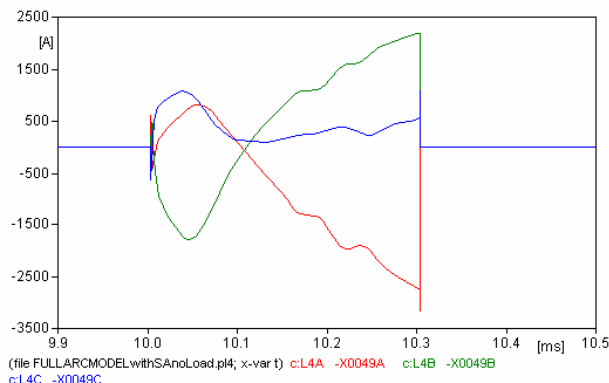**Figure XXIV: Current waveform travelling to the arc on the first pole on the left of point of lightning strike - Sim 1 loaded**
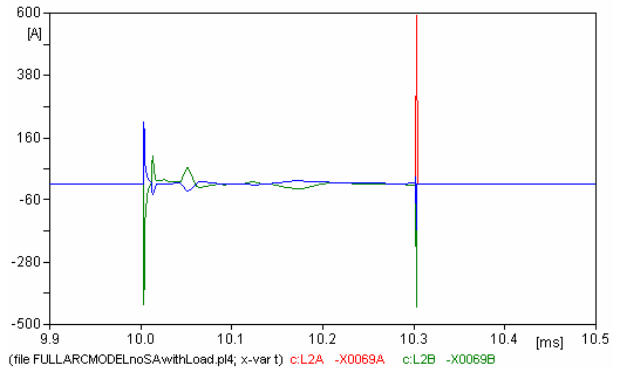
Figure XXV: Current waveform travelling to the arc on the second pole on the left of point of lightning strike - Sim 1 loaded
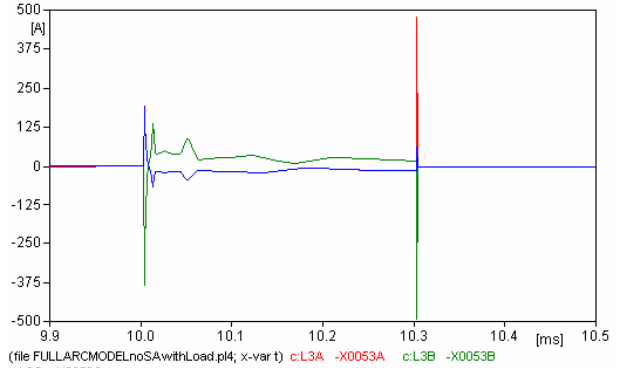
Figure XXVI: Current waveform travelling to the arc on the third pole on the left of point of lightning strike - Sim 1 loaded
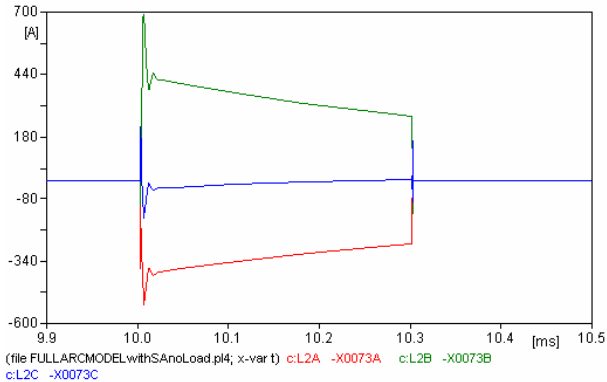

Figure XXVII: Current waveform travelling to the arc on the fourth pole on the left of point of lightning strike - Sim 1 loaded
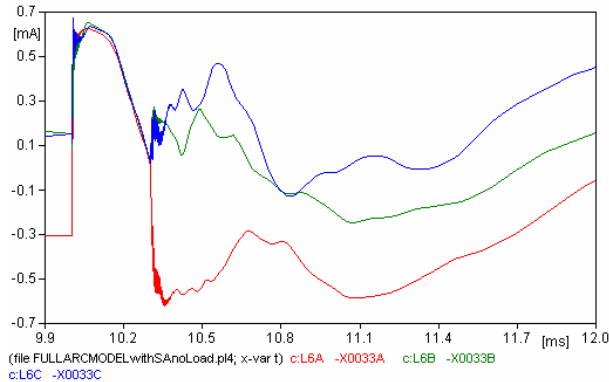
Figure XXVIII: Current waveform travelling to the arc on the fifth pole on the left of point of lightning strike - Sim 1 loaded

Figure XXIX: Current waveform travelling to the arc on the sixth pole on the left of point of lightning strike - Sim 1 loaded
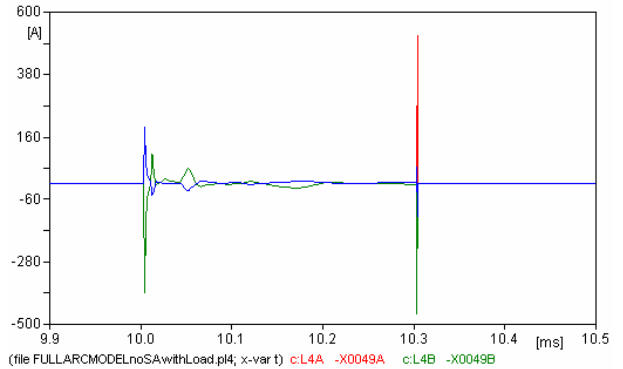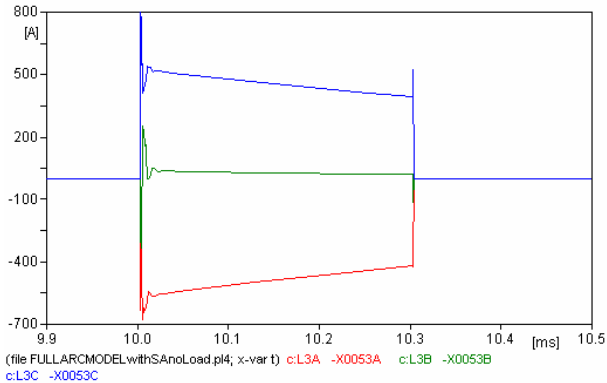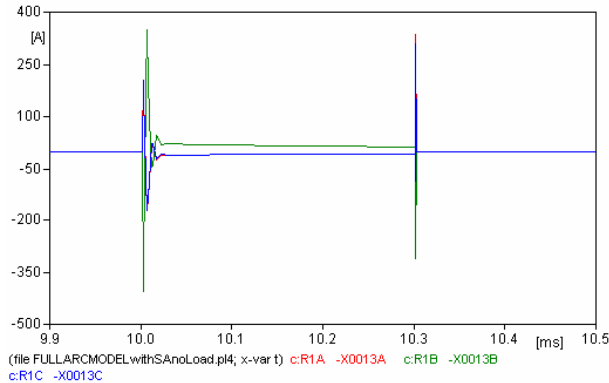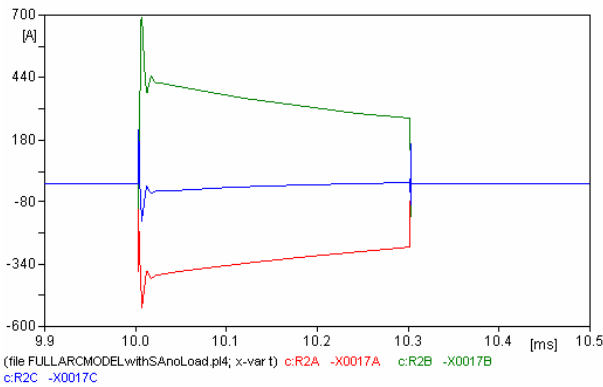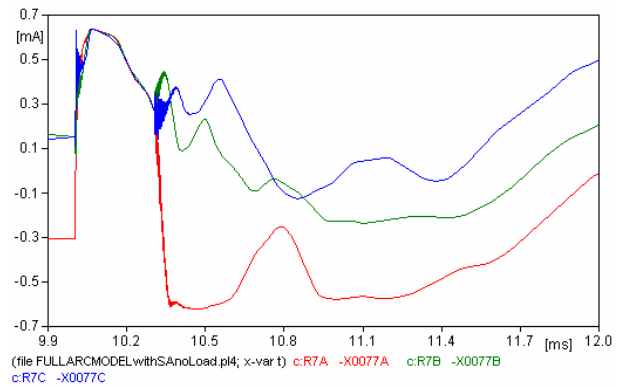

Figure XXX: Current waveform travelling to the arc on the first pole on the right of point of lightning strike - Sim 1 loaded
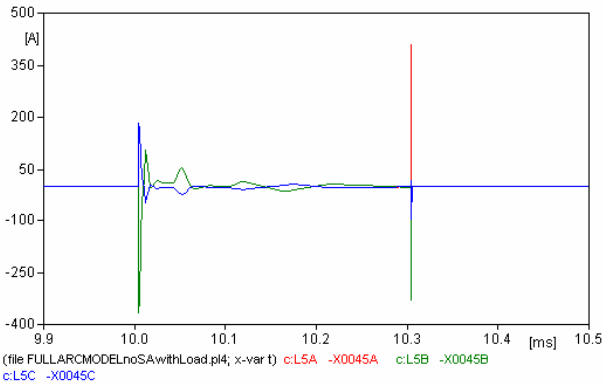
Figure XXXI: Current waveform travelling to the arc on the second pole on the right of point of lightning strike - Sim 1 loaded
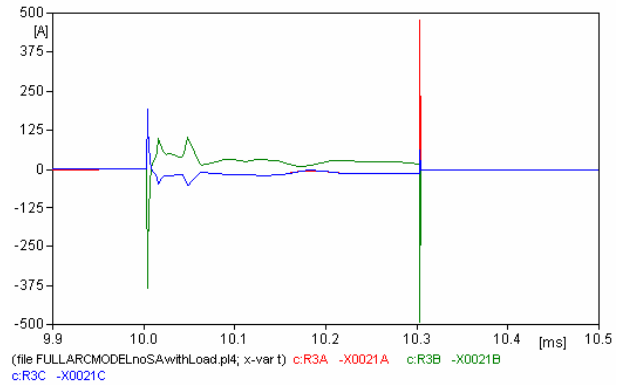
Figure XXXII: Current waveform travelling to the arc on the third pole on the right of point of lightning strike - Sim 1 loaded

Figure XXXIII: Current waveform travelling to the arc on the fourth pole on the right of point of lightning strike - Sim 1 loaded

Figure XXXIV: Current waveform travelling to the arc on the fifth pole on the right of point of lightning strike - Sim 1 loaded

Figure XXXV: Current waveform travelling to the arc on the sixth pole on the right of point of lightning strike - Sim 1 loaded

The second set of figures is of Sim 2 with unloaded transformers.
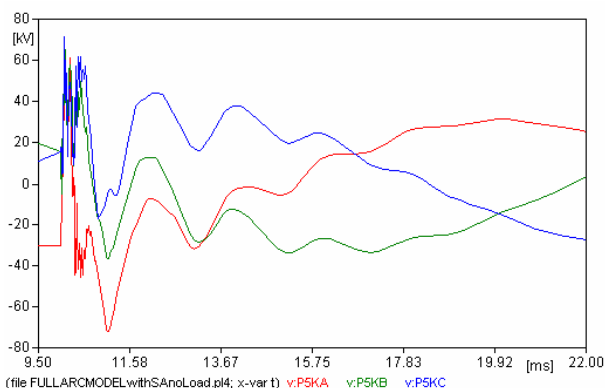
Figure XXXVI: Voltage waveform measurement at the 5 km measurement point on parallel branch 1 - Sim 2 No load
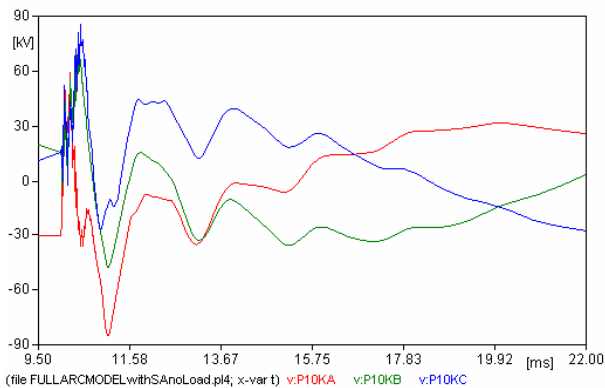
Figure XXXVII: Figure LIV: Voltage waveform measurement at the 10 km measurement point on parallel branch 1 - Sim 2 No load
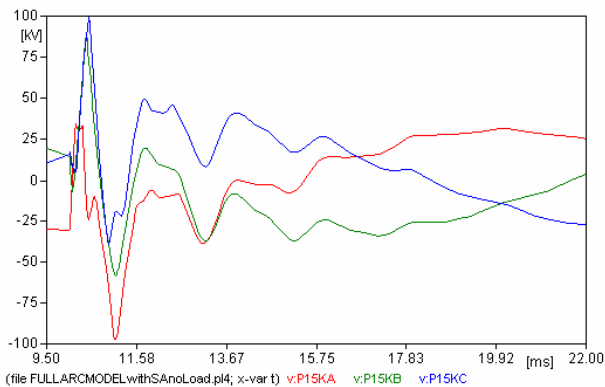
Figure XXXVIII: Figure LIV: Voltage waveform measurement at the 15 km measurement point on parallel branch 1 - Sim 2 No load
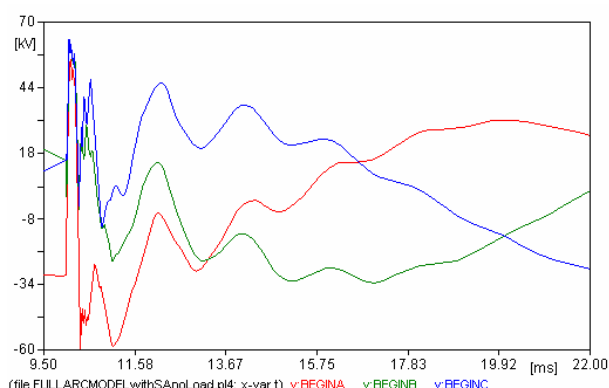
Figure XXXIX: Figure LIV: Voltage waveform measurement at the point of split to the parallel lines - Sim 2 No load

Figure XL:
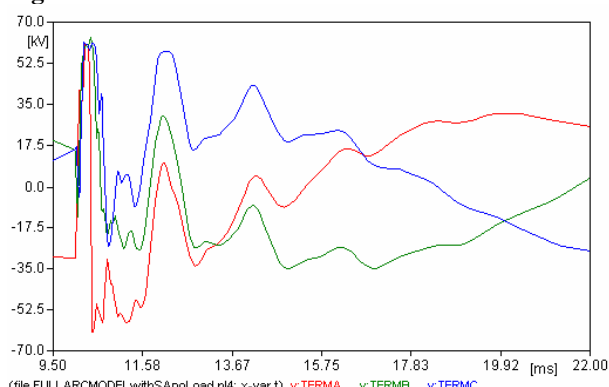
Figure XLI: Voltage waveform measurement at the termination of the main distribution line - Sim 2 No load
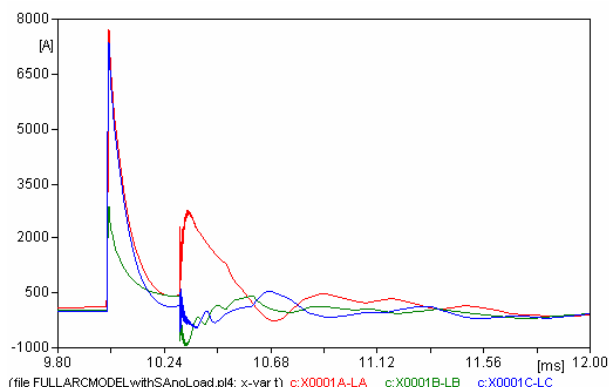
Figure XLII: Current waveform travelling left of the point of lightning strike - Sim 2 No load
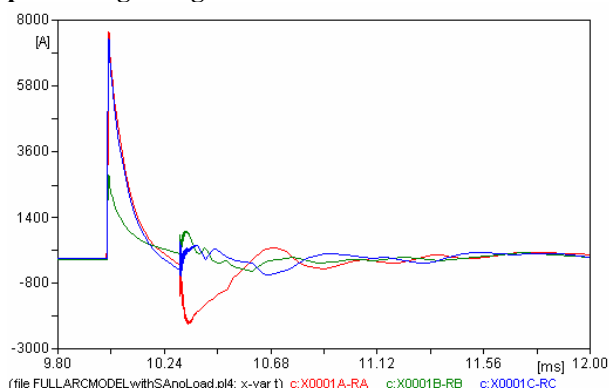
Figure XLIII: Current waveform travelling right of the point of lightning strike - Sim 2 No loa
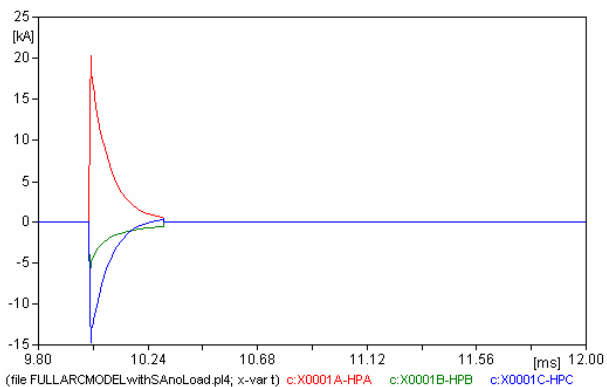
Figure XLIV: Current waveform travelling down the pole nearest the point of lightning strike - Sim 2 No load

Figure XLV: Current waveform travelling to the arc on the first pole on the left of point of lightning strike - Sim 2 No load
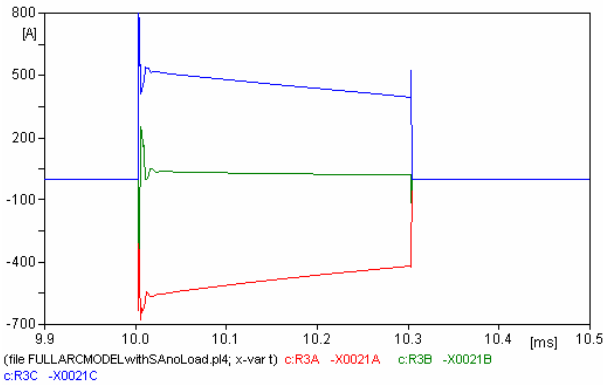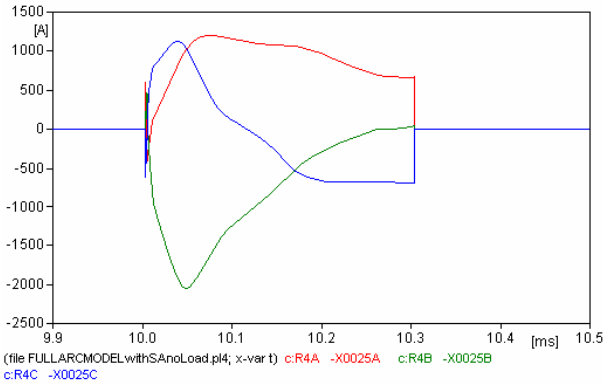

Figure XLVI: Current waveform travelling to the arc on the second pole on the left of point of lightning strike - Sim 2 No load
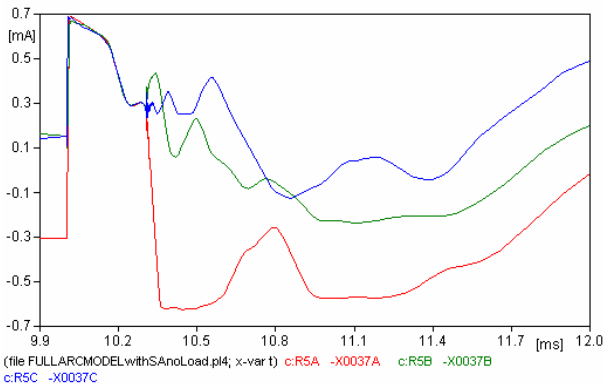

Figure XLVII: Current waveform travelling to the arc on the third pole on the left of point of lightning strike - Sim 2 No load
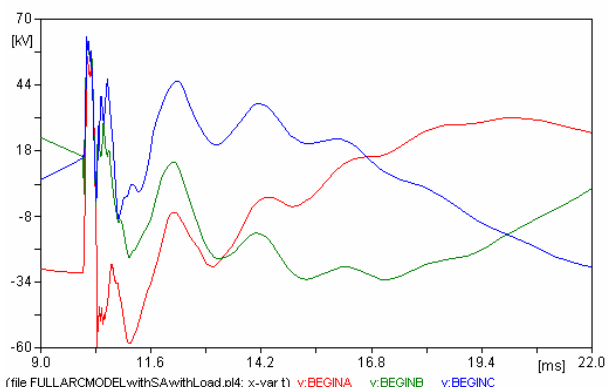

Figure XLVIII: Current waveform travelling to the arc on the fourth pole on the left of point of lightning strike - Sim 2 No load
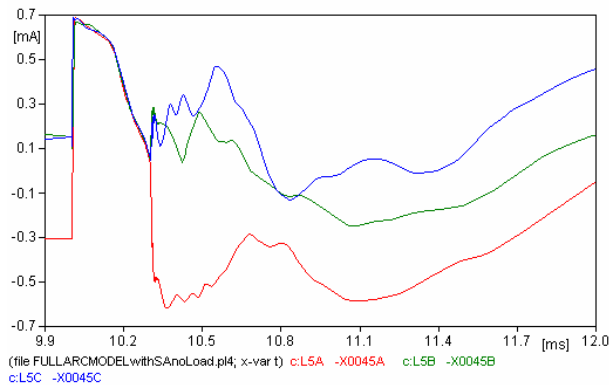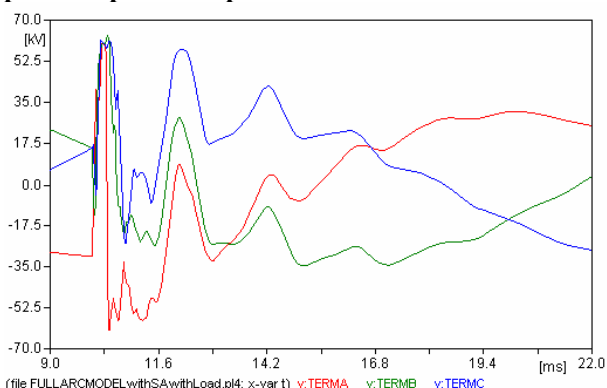

Figure XLIX: Current waveform travelling to the arc on the fifth pole on the left of point of lightning strike - Sim 2 No load
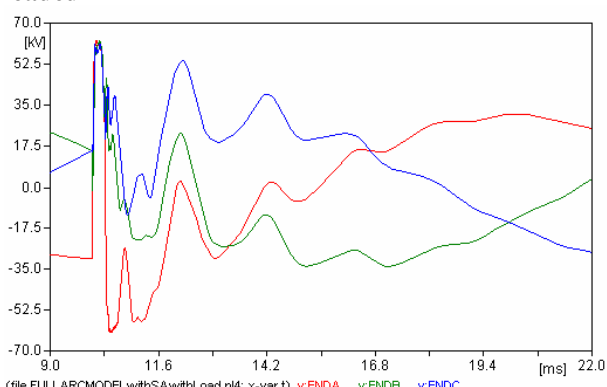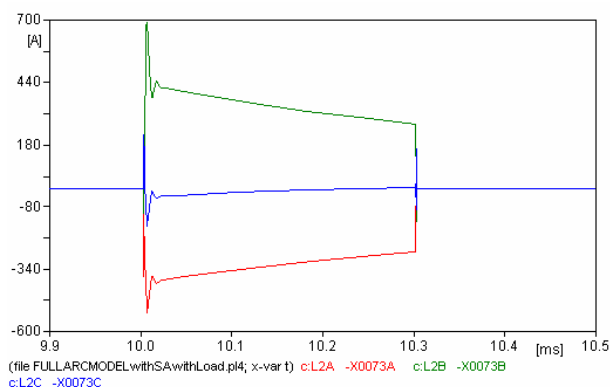

Figure L: Current waveform travelling to the arc on the sixth pole on the left of point of lightning strike - Sim 2 No load

Figure LI: Current waveform travelling to the arc on the first pole on the right of point of lightning strike - Sim 2 No load

Figure LII: Current waveform travelling to the arc on the second pole on the right of point of lightning strike - Sim 2 No load

Figure LVI: Current waveform travelling to the arc on the sixth pole on the right of point of lightning strike - Sim 2 No load

Figure LIII: Current waveform travelling to the arc on the third pole on the right of point of lightning strike - Sim 2 No load

Figure LIV: Current waveform travelling to the arc on the fourth pole on the right of point of lightning strike - Sim 2 No load

Figure LV: Current waveform travelling to the arc on the fifth pole on the right of point of lightning strike - Sim 2 No load

The second set of figures is of Sim 2 with loaded transformers.

Figure LVII: Voltage waveform measurement at the point of split to the parallel lines - Sim 2 loaded

Figure LVIII: Voltage waveform measurement at the termination of the main distribution line - Sim 2 loaded
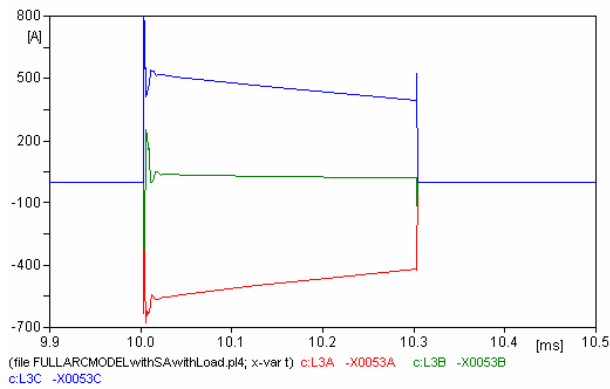

**Figure LIX: Voltage waveform measurement at the end of the main distribution line - Sim 2 loaded**
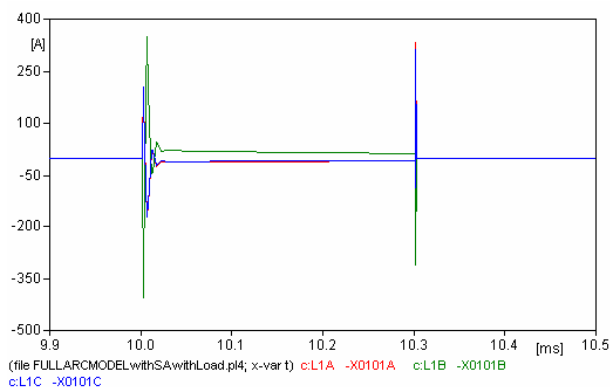
Figure LX: Current waveform travelling to the arc on the first pole on the left of point of lightning strike - Sim 2 loaded

Figure LXI: Current waveform travelling to the arc on the second pole on the left of point of lightning strike - Sim 2 loaded
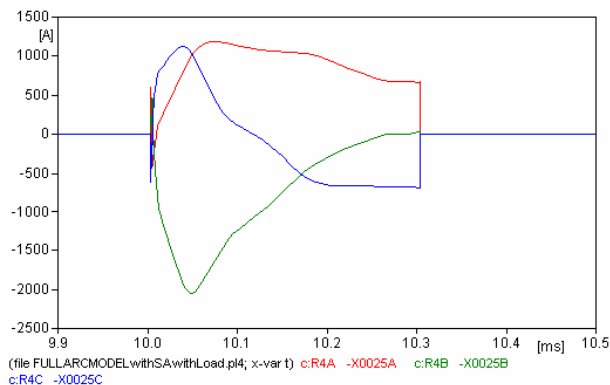

Figure LXII: Current waveform travelling to the arc on the third pole on the left of point of lightning strike - Sim 2 loaded
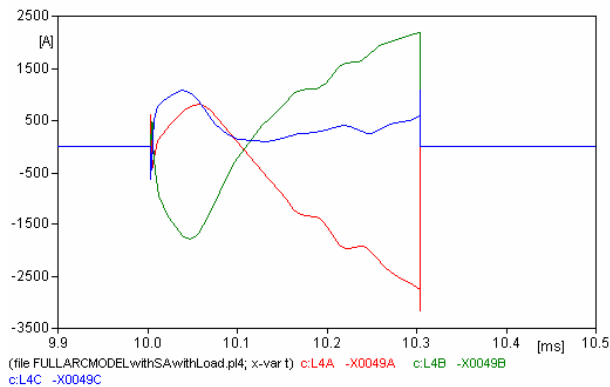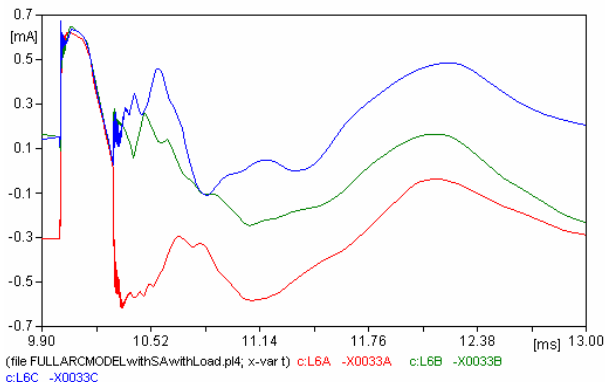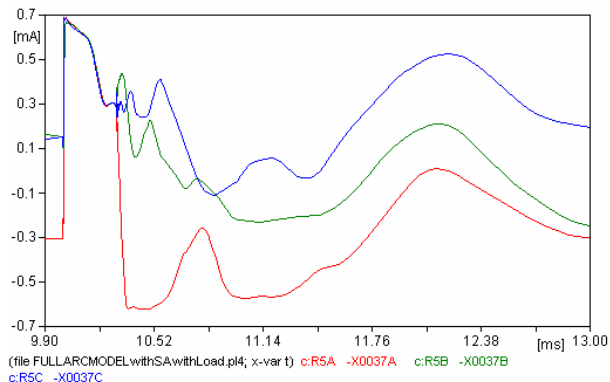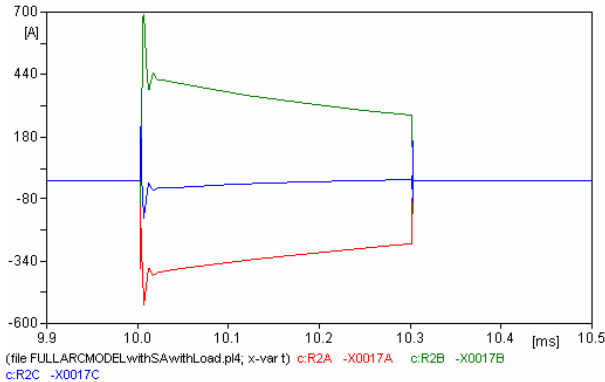

Figure LXIII: Current waveform travelling to the arc on the fourth pole on the left of point of lightning strike - Sim 2 loaded
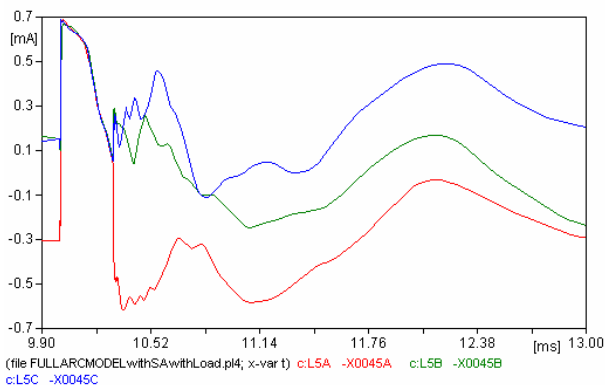
Figure LXIV: Current waveform travelling to the arc on the fifth pole on the left of point of lightning strike - Sim 2 loaded
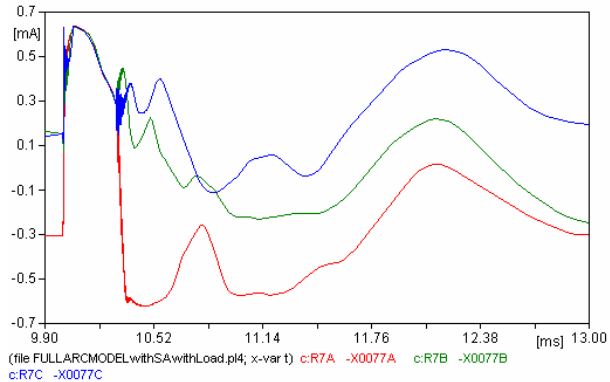

Figure LXV: Current waveform travelling to the arc on the sixth pole on the left of point of lightning strike - Sim 2 loaded
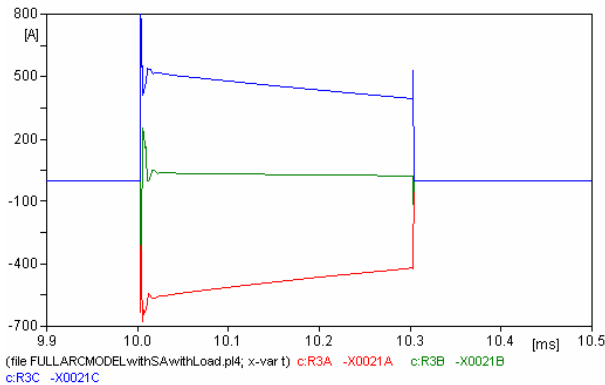

Figure LXVI: Current waveform travelling to the arc on the second pole on the right of point of lightning strike - Sim 2 loaded

Figure LXVII: Current waveform travelling to the arc on the third pole on the right of point of lightning strike - Sim 2 loaded

Figure LXVIII: Current waveform travelling to the arc on the fourth pole on the right of point of lightning strike - Sim 2 loaded

Figure LXIX: Current waveform travelling to the arc on the fifth pole on the right of point of lightning strike - Sim 2 loaded

Figure LXX: Current waveform travelling to the arc on the sixth pole on the right of point of lightning strike - Sim 2 loaded

The diagram below is of the full simulation model. The arc model was compacted and is shown in the next figure in its expanded form.
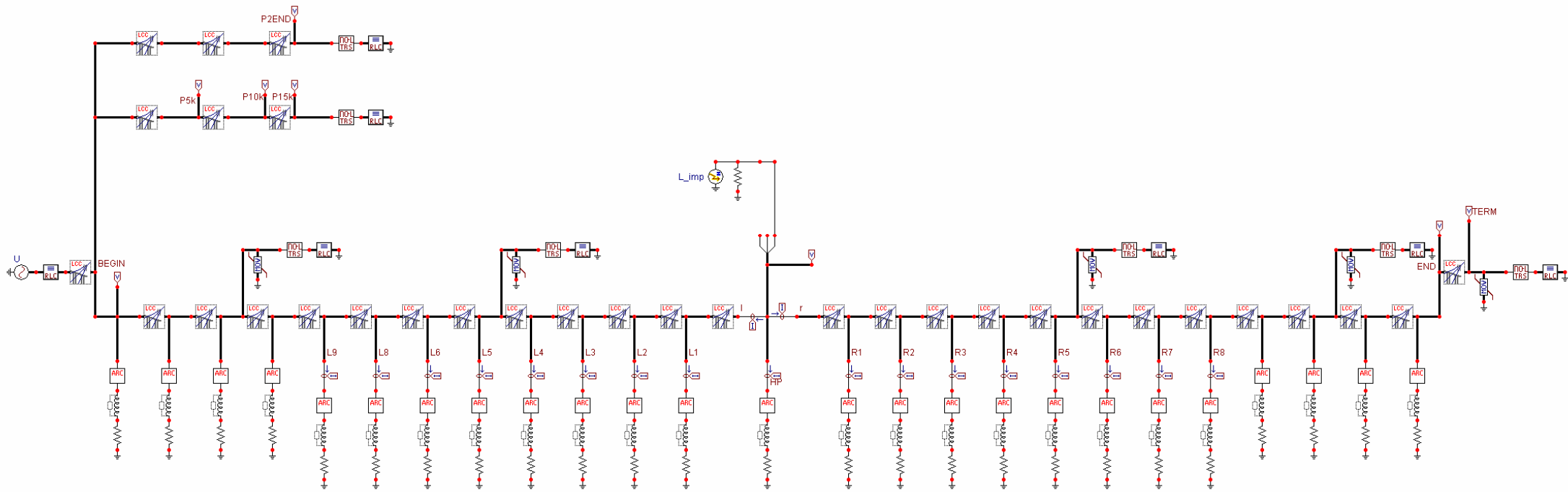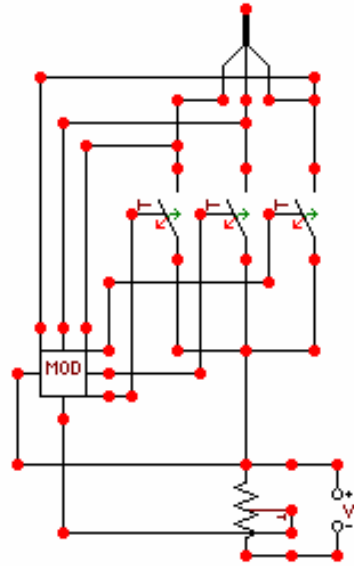

Figure LXXI: Full ATP-EMTP simulation model

Figure LXXII: Contents of "Arc" block from full simulation